63-3-2

Transient Response of a Fluid/Solid Interface due to an Impulsive Pressure Point Source

Freeman Gilbert
Professor of Geophysics

Institute of Geophysics and Planetary Physics
and
Department of Earth Sciences

University of California, San Diego
La Jolla, California

The research reported in this paper was supported by a subcontract with E. H. Plesset Associates, Inc., Engineering Division, Los Angeles, under contract DA-49-146-XZ-073 with the Defense Atomic Support Agency.

First we shall state the problem and give a simple method for its solution. Then we shall describe the empirical method used to relate the solution to the problem of blast loading an air earth interface.

In circular cylindrical coordinates (r, θ, z) a homogeneous, isotropic, solid medium occupies the semi-infinite region $0 \leq z < \infty$, and a homogeneous, isotropic, fluid elastic medium occupies the semi-infinite region $-\infty < z \leq 0$. An impulsive point source of pressure is located at $r = 0$, $z = -h$.

The motion in the solid is a solution to the linear elastic wave equation. Integral expressions for the motion have been derived by Ewing, Jardetzky and Press (Elastic Waves in Layered Media, New York, McGraw-Hill, 1957), Strick ("Propagation of Elastic Wave Motion from an Impulsive Source along a Fluid/Solid Interface", Philosophical Transactions of the Royal Society, Series A, Vol. 251, 1959) and others. Therefore, no derivation of these expressions will be given here.

Let Q be the r component of particle velocity, W be the z component of particle velocity, and T_{zz}, T_{zr}, T_{rr} be the stress components. The Laplace transform with respect to time of these quantities is denoted by an overbar. Consider the problem where the pressure point-source emits a step function of strength M_o at time $t \geq 0$, where $M_o = P_o h$ and where P_o is the pressure amplitude that would occur in an unbounded fluid at distance h from the point-source. Then the integral expressions for the transforms of the motion at r, z are

$$\bar{Q} = \frac{M_o}{\pi i}\int_\Gamma d\rho\, K_1(-s\rho r)\left[\frac{2\rho^3(\eta_s^2-\rho^2)\,e^{-s\eta_\rho z} - 4\rho^2\eta_\rho\eta_s\,e^{-s\eta_s z}}{S(\rho)}\right]e^{-s\eta h} \tag{1.1}$$

$$\bar{W} = \frac{-M_o}{\pi i}\int_\Gamma d\rho\, K_0(-s\rho r)\left[\frac{2\rho\eta_\rho(\eta_s^2-\rho^2)\,e^{-s\eta_\rho z} + 4\rho^3\eta_\rho e^{-s\eta_s z}}{S(\rho)}\right]e^{-s\eta h} \tag{1.2}$$

$$\bar{T}_{zz} = \frac{\mu M_o}{\pi i}\int_\Gamma d\rho\, K_0(-s\rho r)\left[\frac{2\rho(\eta_s^2-\rho^2)^2 e^{-s\eta_\rho z} + 8\rho^3\eta_\rho\eta_s e^{-s\eta_s z}}{S(\rho)}\right]e^{-s\eta h} \tag{1.3}$$

$$\bar{T}_{zr} = \frac{\mu M_o}{\pi i}\int_\Gamma d\rho\, K_1(-s\rho r)\left[\frac{-4\rho^2\eta_\rho(\eta_s^2-\rho^2)}{S(\rho)}\left(e^{-s\eta_\rho z} - e^{-s\eta_s z}\right)\right]e^{-s\eta h} \tag{1.4}$$

$$\begin{aligned}\bar{T}_{rr} = \frac{\mu M_o}{\pi i}\int_\Gamma d\rho \Big\{ & K_0(-s\rho r)\left[\left(-2\lambda\mu^{-1}V_\rho^{-2}\rho(\eta_s^2-\rho^2) + 2\rho^3(\eta_s^2-\rho^2)\right)e^{-s\eta_\rho z}\right. \\ & \left. - 4\rho^3\eta_\rho\eta_s e^{-s\eta_s z}\right] + K_2(-s\rho r)\left[2\rho^3(\eta_s^2-\rho^2)\,e^{-s\eta_\rho z}\right. \\ & \left.\left. - 4\rho^3\eta_\rho\eta_s e^{-s\eta_s z}\right]\right\}\frac{e^{-s\eta h}}{S(\rho)}\end{aligned} \tag{1.5}$$

where $S(p) = \mu\eta\, R(p) + \rho^6 \eta_p \beta^5/\mu$, and $R(p) = (\eta_s^2 - p^2)^2 - 4\eta_s\eta_p p^2$. R(p) is the characteristic Rayleigh denominator in Lamb's problem, and S(p) is the characteristic Stoneley (or Scholte) denominator in Strick's problem. The path of integration, Γ , runs parallel to the imaginary axis between p = 0 and the smaller of $p = v^{-1}$ and $p = v_f^{-1}$.

By considering a step function source, integrals have been obtained in which Laplace transform variable, s, appears only in the exponentials and the argument of the Bessel function. In this case the transformation to the time domain is easily made by operational means. The technique is illustrated by a simple example.

Consider an integral of the form

$$I(s) = \frac{1}{\pi i}\int_\Gamma dp\, K_m(-spr)\, F(p)\, e^{-s\eta_s z - s\eta h} \qquad (2)$$

where F(p) is the ratio of polynomials in p, η_p, η_s, and η . The function $K_n(-spr)$ is the transform of

$$\frac{H(t+pr)\cosh\left[m\cosh^{-1}(t/pr)\right]}{(t^2 - p^2r^2)^{1/2}}$$

and

$$K_m(-spr)\, e^{-s\eta_s z - s\eta h}$$

is the transform of

$$\frac{H(t+pr-\eta_s z-\eta h)\cosh\left(m\cosh^{-1}\left[(t-\eta_s z-\eta h)/pr\right]\right)}{\left[(t-\eta_s z-\eta h)^2 - p^2r^2\right]^{1/2}}$$

Thus the integral I(s) is the transform of

$$I(t) = \frac{1}{\pi i}\int_{\Gamma} \frac{d\rho\, F(\rho)\, H(t+\rho r-\eta_s z-\eta h)\cosh\left(n\cosh^{-1}[(t-\eta_s z-\eta h)/\rho r]\right)}{[(t-\eta_s z-\eta h)^2-\rho^2 r^2]^{1/2}} \tag{3}$$

Let $\tau = -pr + \eta_s z + \eta h$ and deform the path, Γ, in the left half-plane such that on the deformed path τ is real. The deformed path is symmetric with respect to the real axis as in the real part of the integrand so the expression for I(t) can be written

$$I(t) = \frac{2}{\pi}\,\mathrm{Im}\int_{\rho^+} d\rho\, F(\rho)\cdots \tag{4}$$

where p^+ is that part of the deformed path that lies in the second quadrant.

Changing the variable of integration to τ gives

$$I(t) = \frac{2}{\pi}\,\mathrm{Im}\int_{\tau_0}^{t} \frac{d\rho}{d\tau}\, d\tau\, F(\rho)\cdots \tag{5}$$

where p is now regarded as a function of τ, and τ_0 is that value of τ for which the path of integration touches the real p axis.

The problem then is reduced to the numerical evaluation of an integral

$$I(t) = \frac{2}{\pi}\int_{\tau_0}^{t} d\tau\, G(t,\tau) \tag{6}$$

If τ_o corresponds to a real value of p where there is a branch cut, the lower limit of the path of integration is extended toward the origin to the branch point nearest the origin. That value of τ at the branch point is denoted by τ_c, and

$$I(t) = \frac{2}{\pi}\int_{\tau_c}^{\tau_o} d\tau\, G(t,\tau) + \frac{2}{\pi}\int_{\tau_o}^{t} d\tau\, G(t,\tau) \tag{7}$$

If $t < \tau_o$ in (6) or $t < \tau_c$ in (7), I(t) = 0.

For either (6) or (7) it is necessary to evaluate numerically one or more integrals of the type

$$I = \frac{2}{\pi}\int_{\tau_1}^{\tau_2} d\tau\, G(\tau) \tag{8}$$

The method used is the Gauss-Legendre method. First the following transformation is made

$$\tau = \left[(\tau_2^2 - \tau_1^2)\sin^2\theta + \tau_1^2\right]^{1/2}$$

from which is obtained

$$I = \frac{2}{\pi}\int_0^{\pi/2} d\theta\, G(\tau(\theta))\,\frac{(\tau_2^2 - \tau_1^2)\sin\theta\cos\theta}{\tau(\theta)} = \frac{2}{\pi}\int_0^{\pi/2} d\theta\, H(\theta) \tag{9}$$

Next the range of integration is divided into K equal parts, ℓ; $\ell = \pi/2K$;

$$I = \frac{2}{\pi}\sum_{k=1}^{K}\int_{(k-1)\ell}^{k\ell} d\theta\, H(\theta) \tag{10}$$

To this point no approximations have been made.

In the Gauss-Legendre method an integral

$$I' = \int_{\rho}^{\beta} f(y)\, dy$$

is approximated by

$$I' \simeq \frac{\beta-\rho}{2} \sum_{j=1}^{J} a_j f\left(\frac{\beta-\rho}{2} x_j + \frac{\beta+\rho}{2} \right) \tag{11}$$

where x_j is the j^{th} root of the Legendre polynomial $P_J(x)$, $-1 < X < 1$, and a_j is the j^{th} weight.

$$a_j = \frac{1}{P_J'(x_j)} \int_{-1}^{1} \frac{P_J(x)\, dx}{x - x_j} \tag{12}$$

Several tables of weights and roots are available.

The expression for the transformed integral becomes

$$I = \sum_{k=1}^{K} \frac{1}{2K} \sum_{j=1}^{J} a_j\, H\left[(x_j + 2k - 1)\, \ell / 2 \right] \tag{13}$$

The transformation procedure described here has been applied to the integral expressions (1.1) - (1.5) and a FORTRAN program exists for the numerical evaluation of the approximating sums represented by (13).

The five quantities of interest are presented in dimensionless form as follows:

horizontal velocity, $q = \mu Q / P_o v_f$

vertical velocity, $w = \mu W / P_o v_f$

vertical stress, $\tau_{zz} = T_{zz} / P_o$

shear stress, $\tau_{zr} = T_{zr}/P_o$

horizontal stress, $\tau_{rr} = T_{rr}/P_o$

The following compilation defines terms used throughout the above discussion.

ρ^f = density of fluid

ρ^s = density of solid

v_f = acoustic sound speed in fluid

v_p = compressional speed in solid

v_s = shear speed in solid

p = a variable of integration

s = Laplace transform variable

$\eta = (v_f^{-2} - p^2)^{1/2}$

$\eta_p = (v_p^{-2} - p^2)^{1/2}$

$\eta_s = (v_s^{-2} - p^2)$

These expressions are multivalued functions of p. To render them, and expressions involving them, single valued, branch cuts are introduced, in the case of η, from $p = v_f^{-1}$ to $p = \infty$ and from $p = -v_f^{-1}$ to $p = -\infty$.

$K_n(\alpha)$ = modified Bessel function of the second kind, or order n and argument α.

μ = rigidity modulus of solid.

The results obtained above represent a solution to the linear elastic wave equation. In order to use the results to study the problem of blast loading an air/earth interface, several simplifying assumptions must be made. First, it was decided to consider the response at four ranges, corresponding to pressure levels of 10,000,5000, 1000, and 500 psi. The parameter P_o should be larger than the largest pressure considered and was arbitrarily chosen to be 20,000 psi. That is to say, at a distance h from the point source the pressure would be 20,000 psi when the solid half-space is absent. The ranges corresponding to the four pressure levels considered were taken from the data of Brode (RAND, P-1951, March 1960). Then for each pressure level the parameter h was chosen such that the incident pressure field would have the proper value. For a pressure P at range r we have

$$P = hP_o/(h^2 + r^2)^{1/2}$$

For a given P and r and with P_o = 20,000 psi h can be determined. Thus h is different for each pressure level and can be regarded as the "effective" height of burst.

The horizontal blast wave velocity was taken from the data of Brode and from it an "effective" fluid speed can be calculated for each range.

Finally, the density of the fluid is taken to be the density behind the blast wavefront in the Brode data and therefore is also a function of range. This last assumption is not very important since the fluid/solid density contrast is always very large.

On this basis several problems were solved. Ground materials considered were "rock" (dilatational velocity c_p = 15,000 ft/sec, shear velocity c_s = 8,000 ft/sec, unit weight γ = 170 lb/ft^3), "tuff" (c_p = 7,900 ft/sec, c_s = 4,000 ft/sec, γ = 130 lb/ft^3), "sediment" (c_p = 2,400 ft/sec, c_s = 800 ft/sec, γ = 120 lb/ft^3) and "dirt" (c_p = 800 ft/sec, c_s = 200 ft/sec, γ = 100 lb/ft^3). Pressure levels considered were 10,000, 5,000, 1,000 and 500 psi; depths investigated were 0, 40 and 80 feet. Horizontal and vertical normal stresses, shear stress, and horizontal and vertical velocities were computed. Results for tuff are included in this presentation; results for rock and sediment are given in Appendix A. Extreme requirements of computer time prevented extending the curves for dirt to times at which the Rayleigh wave phenomena would occur; therefore, no results for dirt are given.

The Rayleigh wave contribution is not apparent from examination of the stress and velocity curves; the most satisfactory method of identifying the Rayleigh wave is by examination of particle motions. The Rayleigh wave is unique in that particle motion is retrograde with respect to the solid half-space. Particle paths are shown in Figure 12 for surface points at the four overpressure levels. Since the velocity curves of Figures 10 and 11 begin at the time corresponding to the peak stress traveling directly through the fluid (i.e., at 188 ms) early-time motions are not shown. The vertical velocity increases abruptly after the fluid pulse arrival while the horizontal velocity decreases equally rapidly. Positive directions of vertical and horizontal velocities are upward and outward, respectively. Therefore, the motions following the arrival of the fluid wave are retrograde and identify the passage of the Rayleigh wave.

Once this wave is located for one pressure level it can be identified quite readily at the other pressure levels as well; therefore it is necessary only to examine velocity curves at one overpressure level. For tuff the sharp downward thrust of the horizontal stress curves immediately following the initial peak is caused by the Rayleigh wave. The relative importance of the Rayleigh wave at the four overpressure levels can be seen quite clearly. At 500 psi (nominal) the Rayleigh wave horizontal stress is of much greater absolute magnitude than that from the fluid pulse. However, since the stresses from these two wave arrivals are opposite in sign the net result of these effects is a positive stress arising from the fluid pulse. As overpressures increase the Rayleigh wave horizontal stresses become less important; for P_{so} = 5,000 and 10,000 psi the Rayleigh wave effect is not of sufficient magnitude to cause these stresses to become positive.

The Rayleigh wave has far less effect on vertical stress than on horizontal stress. For surface stresses no effects are shown whereas the effects for depths of 40 and 80 feet are less than 10 percent greater for P_{so} = 500 psi and less than 3 percent greater for P_{so} = 10,000 psi. Shear stress effects become quite large, particularly at lower pressure levels, as evidenced by Figure 9.

The pattern of stresses which follows the Rayleigh wave peak horizontal stress is at least partially obscured by oscillations of the numerical evaluation. This is particularly apparent in the horizontal stress curves for P_{so} = 5,000, 1,000 and 500 psi. Similar oscillations appear in the vertical and shear stress curves and also in the vertical and horizontal velocity curves. Such fluctuations could have been

eliminated by choosing shorter time steps at later times. This was not undertaken in the present study because these oscillations did not impair the usefulness of the results in defining Rayleigh wave effects.

After the passage of the Rayleigh wave, vertical stresses for depths of 40 and 80 feet tend toward the values of surface stresses. Surface stresses, in turn, have stabilized at a value equal to the constant-valued fluid pressure at these later times. However, horizontal stresses for all depths increase negatively, by a large amount and, in the cases of P_{so} = 10,000 and 5,000 psi, become larger than at the time of passage of the fluid pulse. For P_{so} = 10,000 psi these later stresses are almost 40 percent greater than those associated with the fluid compressional wave. It can be established that these late time horizontal stresses are not a result of the Rayleigh wave disturbance by examining the particle motion curves of Figure 12. The transition from retrograde to prograde motion can be seen clearly. As indicated in this figure the change occurs at a time corresponding to that of the peak Rayleigh wave stress for each pressure level considered.

For the most part only qualitative conclusions can be drawn from the above results (and those given in Appendix A) because of the simplifications involved in the analysis. The most important of the simplifying assumptions is that of a non-decaying pulse. Were the pressure source a decaying pulse similar to the Brode air blast pulse, vertical stresses would exhibit a sharp decay following the initial peak. The horizontal stresses also would show such a decay but this would be seen primarily at times after the occurrence of the Rayleigh wave peak stress. It is unlikely that a decaying pulse would give rise to great changes in the

relative magnitudes of the first peak and the Rayleigh wave peak stress. Therefore, the above comments regarding the relative importance of the Rayleigh wave at various overpressure levels appear to be valid.

On this basis it may be stated that, for stresses in tuff at least, the Rayleigh wave is of less importance than are the other "air"-induced effects in the close-in region (i.e., above 1,000 psi). This statement must be qualified by adding that, taken alone, the Rayleigh waye effects surpass the air-induced effects; however, the phasing of the two effects is such that the Rayleigh wave stresses are opposite in sign to those which exist prior to the Rayleigh wave arrival. Therefore, the net effect of the Rayleigh wave is a reduction in stress rather than an increase. Since this phasing is the dominant factor in determining Rayleigh wave effects these results are at odds with the assumption, on which some earlier analyses were based, that the Rayleigh wave effects may be described independently of the other air-induced effects.

APPENDIX A

The cases studied included four ground materials (rock, tuff, sediment, and dirt), four overpressure levels, (10,000, 5,000, 1,000 and 500 psi) and three depths (0, 40 and 80 feet). Properties assigned to the ground materials were in terms of dilatational wave velocity, c_p, and shear wave velocity c_s. Values used were as follows: for rock, c_p = 15,000 ft/sec, c_s = 8,000 ft/sec; for tuff, c_p = 7,900 ft/sec, c_s = 4,000 ft/sec; for sediment, c_p = 2,400 ft/sec, c_s = 800 ft/sec; for dirt, c_p = 800 ft/sec, c_s = 200 ft/sec. Corresponding values of Poisson's ratio are 0.30 for rock, 0.33 for tuff, 0.43 for sediment, and 0.47 for dirt. Results, in the form of time histories of vertical and horizontal stresses and velocities, are given here for rock and sediment. Results for tuff are given in the main text. No results are given for dirt; excessive computation time requirements prevented extending these results to times at which the Rayleigh wave disturbance would occur.

The timewise location of the Rayleigh wave is best detected from inspection of the particle motion, which is uniquely retrograde during passage of the Rayleigh wave. This has been accomplished primarily from direct study of velocity data although motion calculations were helpful. Identification of the Rayleigh wave by means of motion graphs is discussed in the main text and shown in Figure 12.

Results for rock and sediment are shown in Figures A-1 through A-10 and A-11 through A-20, respectively; those for tuff are given in the main text.

Examination of the rock particle velocity curves of Figures A-9 and A-10 for P_{so} = 1,000 psi shows that the retrograde motion associated with the Rayleigh wave pulse begins at about 192 ms, at which time the vertical particle velocity changes sign. In Figure A-7, in which are presented results for horizontal stresses for P_{so} = 1,000 psi, the pulse thus identified can be seen to peak at 200 ms. At 500 psi (Figure A-8) the peak can be seen to occur at 260 ms, whereas the curves for 10,000 and 5,000 psi (Figures A-5 and A-6) show the peak to occur at 80 and 100 ms, respectively. In these figures the Rayleigh wave contribution to the horizontal stress appears to have a somewhat more rounded shape than in Figure A-7 and A-8. This is largely a matter of the scales chosen for the abscissas of these graphs; drawn to the same scale the curves of Figures A-6 and A-7 would appear much less rounded.

It is apparent from these figures that the relative importance of the Rayleigh wave contribution to horizontal stress in rock is most important at the lower overpressures. In each case the Rayleigh wave produces horizontal stresses opposite in direction to those of the pulse which is associated with the passage of the fluid pulse front. These horizontal stress curves for tuff and sediment also show decreasing Rayleigh wave importance with increasing pressure and Rayleigh wave stresses opposite in direction to those from the dilatational wave.

It is useful to discuss further the relative velocities of the fluid and solid elastic waves. For rock the fluid pulse is superseismic (i.e., the point of intersection of the fluid wave front ant the solid surface travels at a velocity greater than the propagation speed of dilatational waves in the solid) for nominal pressure levels of 10,000

and 5,000 psi. For P_{so} = 1,000 psi the fluid pulse is transseismic (i.e., its velocity lies between that of dilatational and shear waves in the solid) and for P_{so} = 500 psi it is subseismic (i.e., its velocity is less than that of shear waves in the solid). At both 1,000 psi and 500 psi the fluid pulse velocity is relatively close to that of the shear wave velocity; the fluid and dilatational wave velocities are fairly close for P_{so} = 10,000, 5,000 and 1,000 psi and transseismic for P_{so} = 500 psi. The dilatational and fluid wave velocities are very closely matched at 500 psi and relatively close at 1,000 psi. The fluid pulse is strongly superseismic in all cases for sediment.

In terms of the relative velocities it may be stated from the horizontal stress results that the Rayleigh wave contribution is not of great importance in the superseismic situation even when the fluid velocity closely approaches that of dilatational waves in the solid. The contribution is large in both the transseismic and subseismic regions and reaches its greatest importance when the fluid wave velocity closely approaches that of the solid shear wave.

Horizontal stress curves for P_{so} = 10,000 and 5,000 psi for both rock and tuff show a rapid rise to a first peak* associated with the passage of the fluid pulse. This is followed by a steep decay upon arrival of the Rayleigh wave followed in turn by a later increase as the Rayleigh wave passes. The horizontal stress curves for tuff at 1,000 and 500 psi also follow this pattern. The first arrival shown in Figure A-7, for rock at 1,000 psi is not that of the fluid equivalent of the air-blast shock front. The arrival time of this early disturbance corresponds to that of a dilatational wave induced directly

*In this discussion a more-negative (i.e., compressive) stress is considered greater than a less-negative stress.

beneath the burst. The fluid wave front arrives at 188 ms, when the pulse has gone positive by an extremely large amount. The Rayleigh wave peak occurs at 200 ms and gives the most positive point on the curve for each depth. In Figure A-8, for rock at 500 psi the fluid pulse arrives after the positive peak; the effect of this pulse can be seen in the abrupt change of the surface stress from 4,350 to 2,300 psi in about 10 ms. In this case the Rayleigh wave peak occurs at 260 ms and the first arrival is that of a dilatational wave induced directly beneath the pulse. It is apparent that the surface disturbance has outrun the fluid wave.

The critical situation in rock is shown in Figure A-7 for P_{so} = 1,000 psi where the fluid pulse is passing from the transseismic to the subseismic case. This only occurs in the region of interest for materials of high seismic velocity such as the rock considered here; even for tuff the location of this transition is far beyond the distance for which P_{so} = 1,000 psi. Such high-velocity materials also possess great strength and high modulus of elasticity. Such materials are far more able to withstand the large stresses associated with the Rayleigh wave in the transseismic region than are softer materials. Thus horizontal stress effects appear to be largest in materials which are best suited to supporting such stresses. There is, of course, some question as to the significance relative to design of the high-intensity tensile stresses such as those of Figure A-7 (i.e., 4,000 psi).

The absolute magnitude of horizontal stress in rock arising from the passage of the Rayleigh wave is in no instance greater than the peak fluid induced horizontal stress at P_{so} = 10,000 psi. For tuff the Rayleigh

wave stress is nowhere larger than the fluid-induced stress at P_{so} = 1,000 psi. Results for sediment are incapable of supporting such a statement directly because the computations were halted before the Rayleigh wave peak occurred for P_{so} = 1,000 and 500 psi. Comparison of the sediment curves for horizontal velocity with those for rock and tuff at P_{so} = 10,000 and 5,000 psi indicates that the Rayleigh wave effects for sediment are less important relative to the fluid-induced effects than are the effects in rock or tuff.

Surface vertical stress curves for rock at all pressure levels show an abrupt rise on arrival of the fluid pulse and a constant value of stress thereafter. Stress curves for depths of 40 and 80 feet closely approximate the surface curves for P_{so} = 10,000 and 5,000 psi; for P_{so} = 1,000 and 500 psi the 40 and 80 feet curves differ considerably from the surface curves at earlier times. These differences at early times are attributable to the outrunning ground shock at these lower pressure levels. At 1,000 psi the early stresses are insignificant relative to the stresses which occur after the fluid pulse arrival. The relative importance of the early stresses is greater for P_{so} = 500 psi but fluid pulse stresses remain greater than those associated with the Rayleigh wave. The Rayleigh wave effects in each case tend to counter the stresses from the fluid pulse. At later times curves for all depths tend toward the value of surface pressure, as is to be expected.

Curves for vertical stresses in tuff and sediment exhibit the same patterns as those for rock with the exception that no outrunning occurs for these softer materials. Sediment results for later times at P_{so} = 1,000 and 500 psi are unavailable but the results appear to follow those for tuff.

Velocity curves for rock are shown in Figures A-9 and A-10 for vertical and horizontal velocity, respectively. For sediment the corresponding figures are A-19 and A-20 and for tuff, Figures 10 and 11 of the main text. Motion phenomena are strongly affected by the shape of the pulse and no comments regarding magnitudes of the velocities are in order. These curves are useful primarily in identifying the Rayleigh wave from the retrograde motion. This motion can be found readily by considering simultaneously the changes in vertical and horizontal motion.

Because of the simplifications involved in this analysis of the Rayleigh wave only limited conclusions are drawn. These are sufficient to define the relative importance of the Rayleigh wave contribution, at least with regard to stresses. These conclusions are as follows: 1.) The Rayleigh wave is never of primary importance for horizontal stresses in the superseismic case; therefore, only materials having seismic velocities greater than 8,300 ft/sec (the air-blast wave velocity at P_{so} = 1,000 psi) will exhibit important Rayleigh wave effects in the close-in region. 2.) The Rayleigh wave is never of great importance for vertical stresses at any location for any material. 3.) The Rayleigh wave horizontal stresses are opposite in sign to those accompanying the air blast wave and tend to reduce the effects of the latter; for vertical stresses the results generally are additive but the Rayleigh wave contribution is of minor importance. 4.) When Rayleigh wave effects are important the stresses involved are tensile.

Based on the above conclusions stresses arising from the Rayleigh wave appear to be of less importance than are other air-induced effects

in the close-in region and can be neglected for most design applications without introducing appreciable error into the analysis. In order to make a comparable statement regarding ground motions it will be necessary to base any future analysis on a more realistic representation of the air blast pulse.

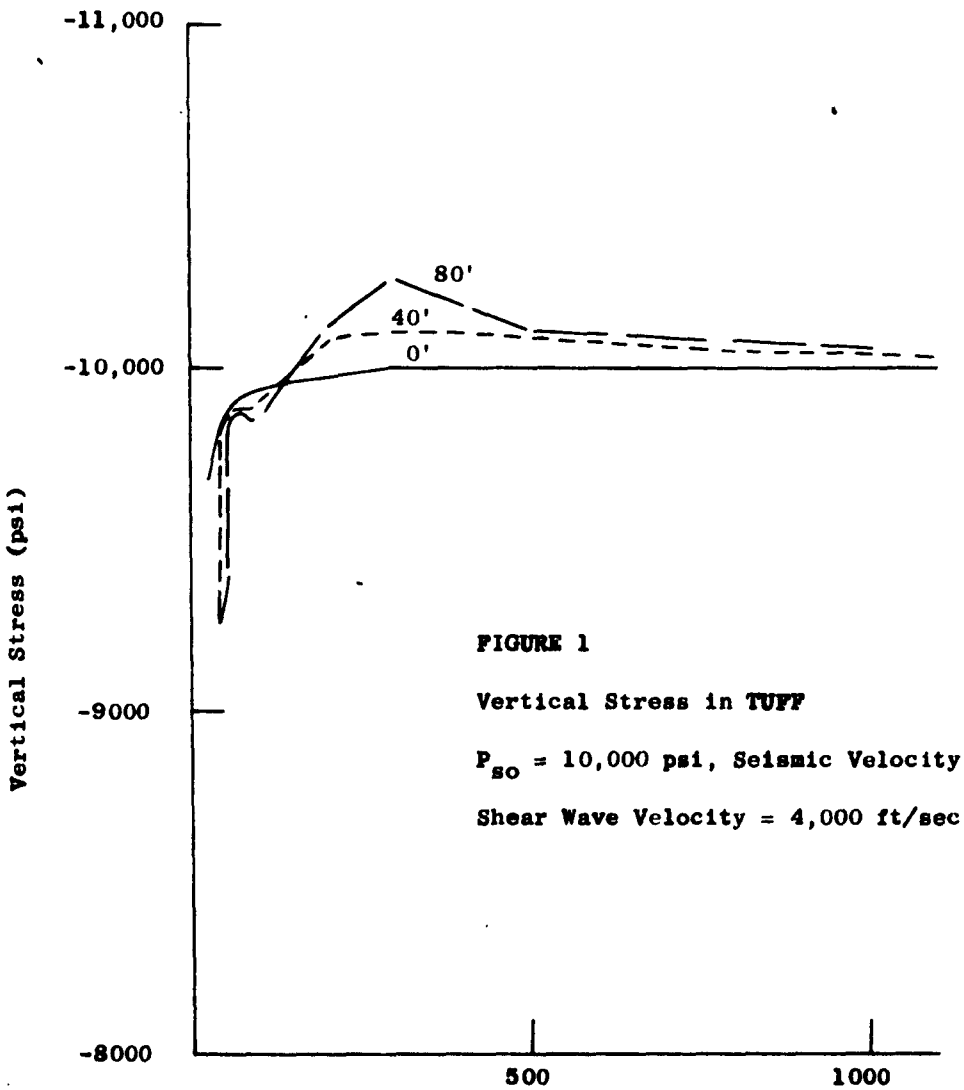

FIGURE 1

Vertical Stress in TUFF

P_{so} = 10,000 psi, Seismic Velocity = 7,900 ft/sec.

Shear Wave Velocity = 4,000 ft/sec.

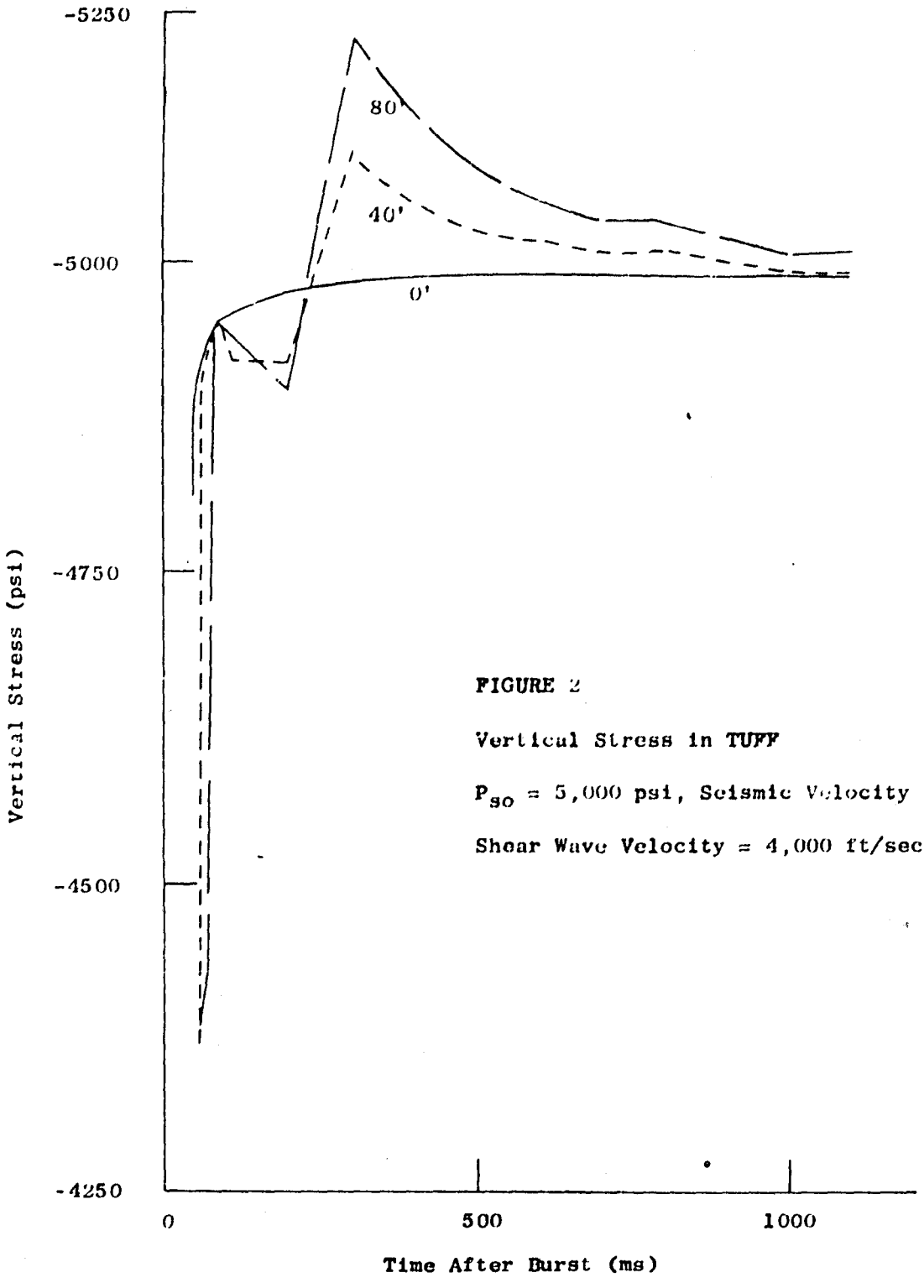

FIGURE 2

Vertical Stress in TUFF

P_{so} = 5,000 psi, Seismic Velocity = 7,900 ft/sec.

Shear Wave Velocity = 4,000 ft/sec.

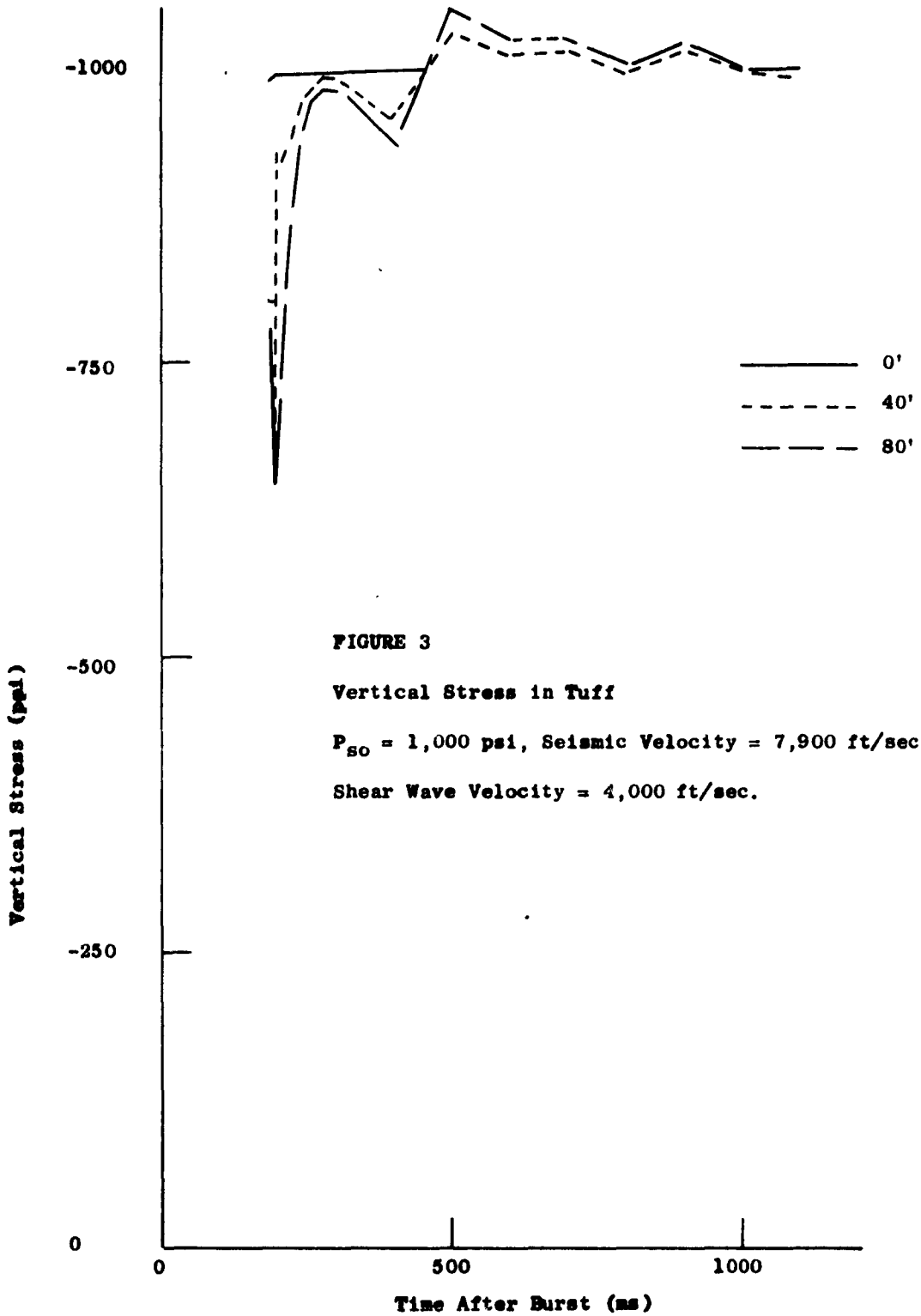

FIGURE 3

Vertical Stress in Tuff

P_{so} = 1,000 psi, Seismic Velocity = 7,900 ft/sec

Shear Wave Velocity = 4,000 ft/sec.

FIGURE 4

Vertical Stress in Tuff

P_{so} = 500 psi, Seismic Velocity = 7,900 ft/sec

Shear Wave Velocity = 4,000 ft/sec

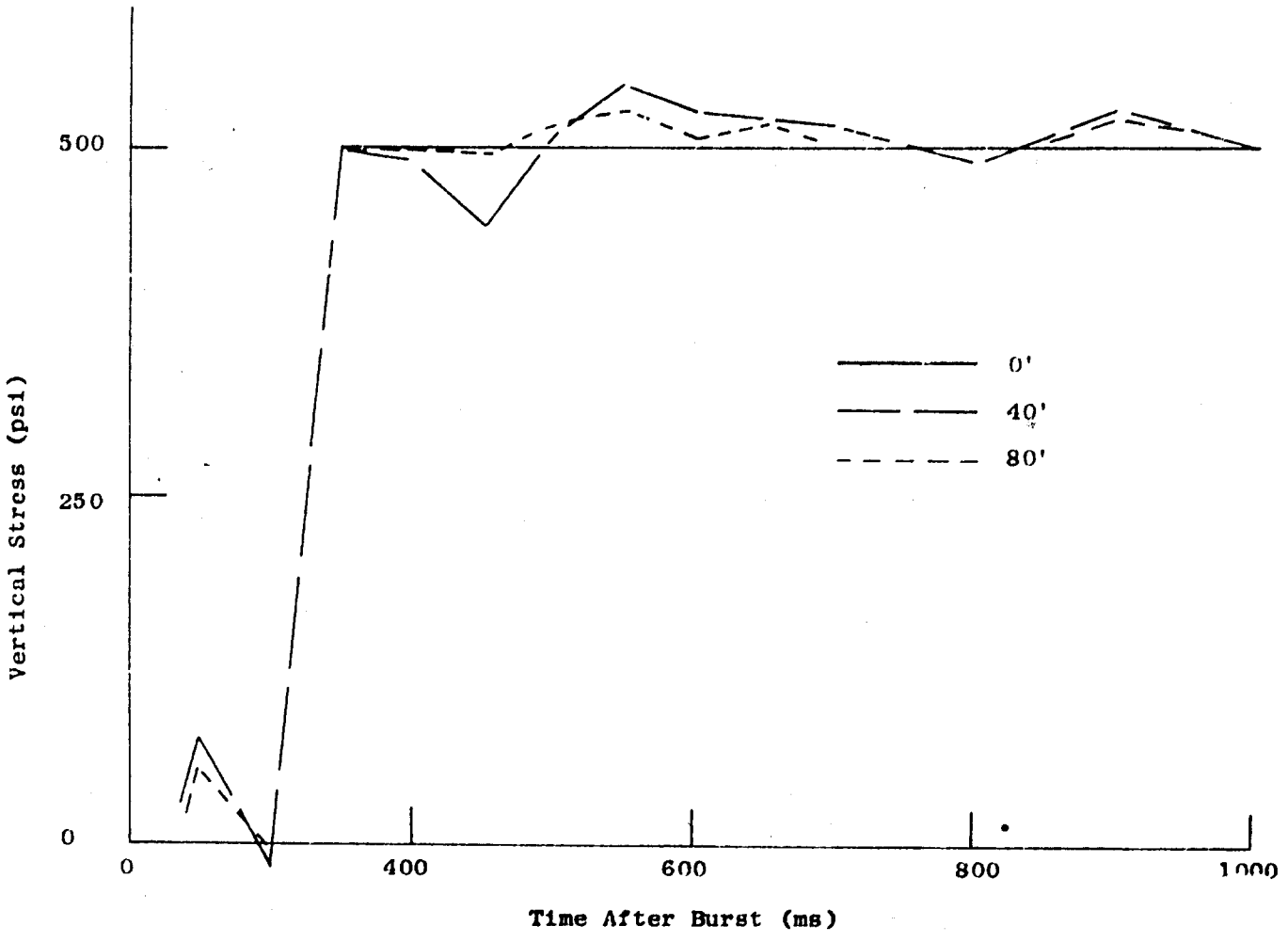

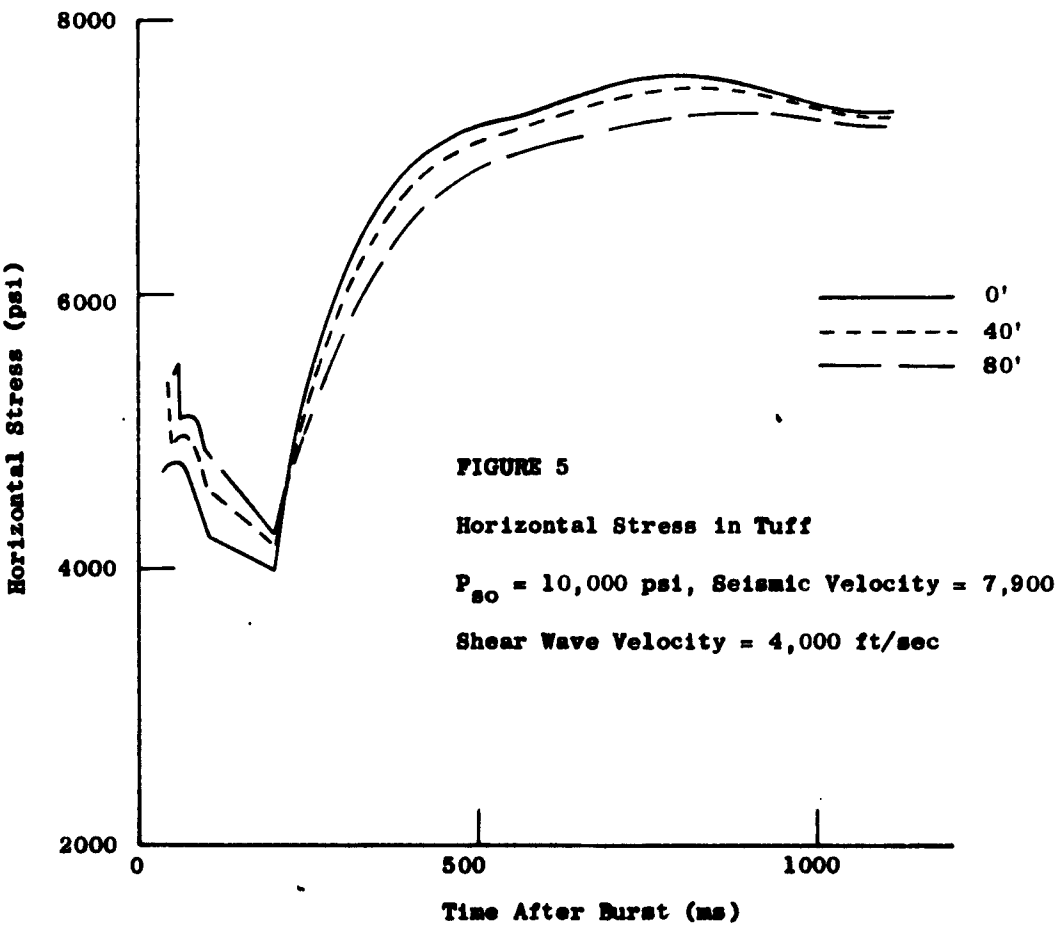

FIGURE 5

Horizontal Stress in Tuff

P_{so} = 10,000 psi, Seismic Velocity = 7,900 ft/sec

Shear Wave Velocity = 4,000 ft/sec

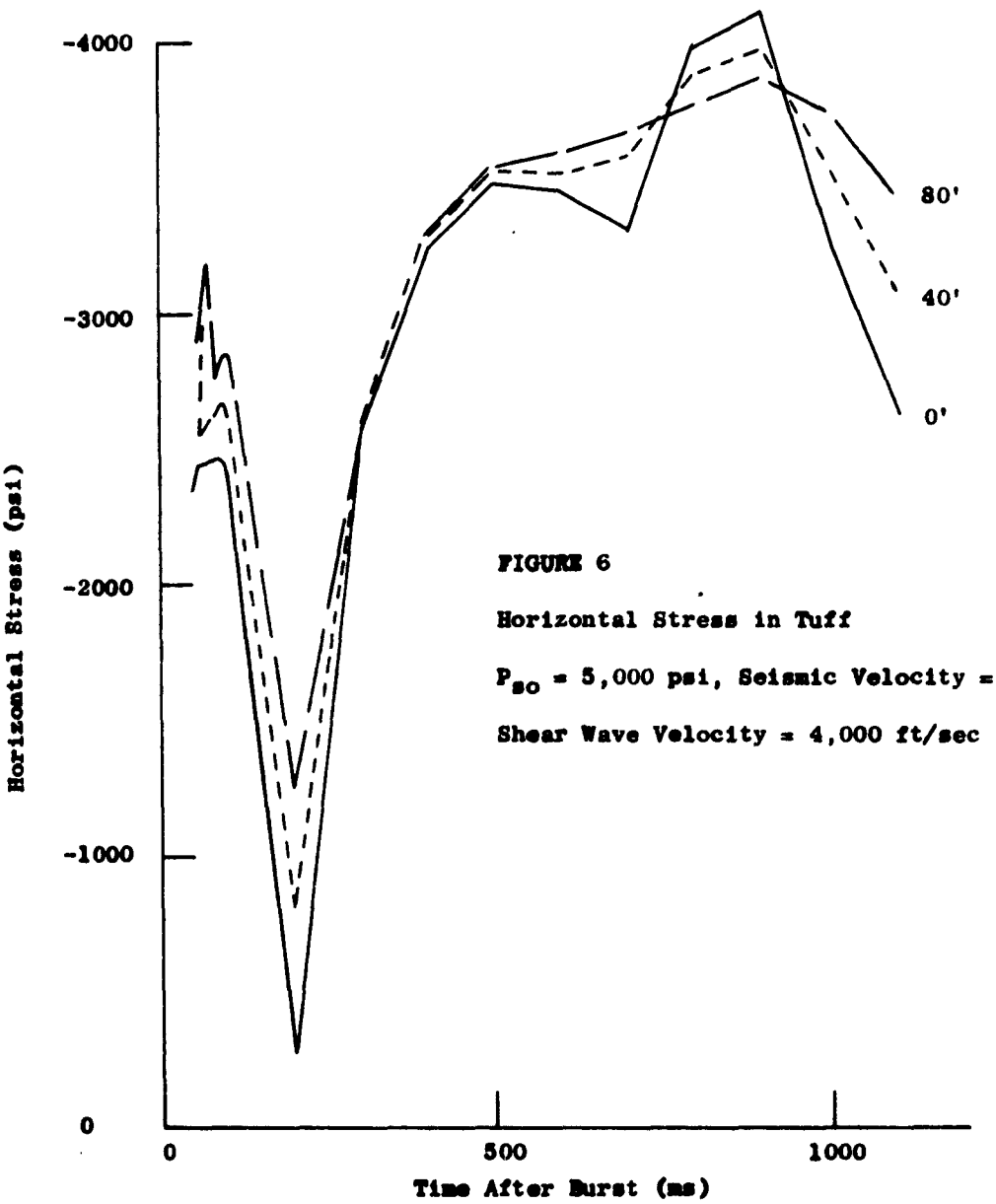

FIGURE 6

Horizontal Stress in Tuff

P_{so} = 5,000 psi, Seismic Velocity = 7,900 ft/sec

Shear Wave Velocity = 4,000 ft/sec

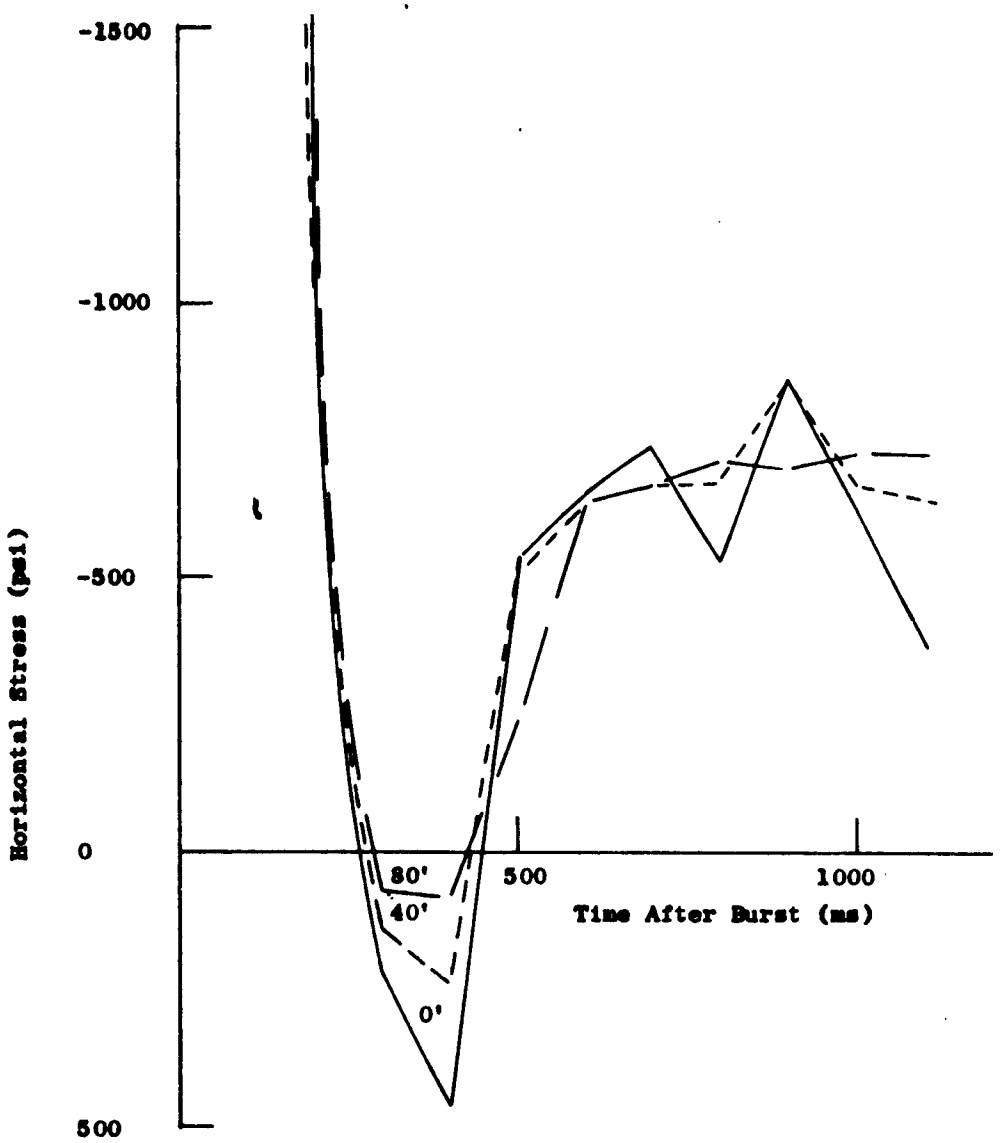

FIGURE 7

Horizontal Stress in Tuff

P_{so} = 1,000 psi, Seismic Velocity = 7,900 ft/sec

Shear Wave Velocity = 4,000 ft/sec

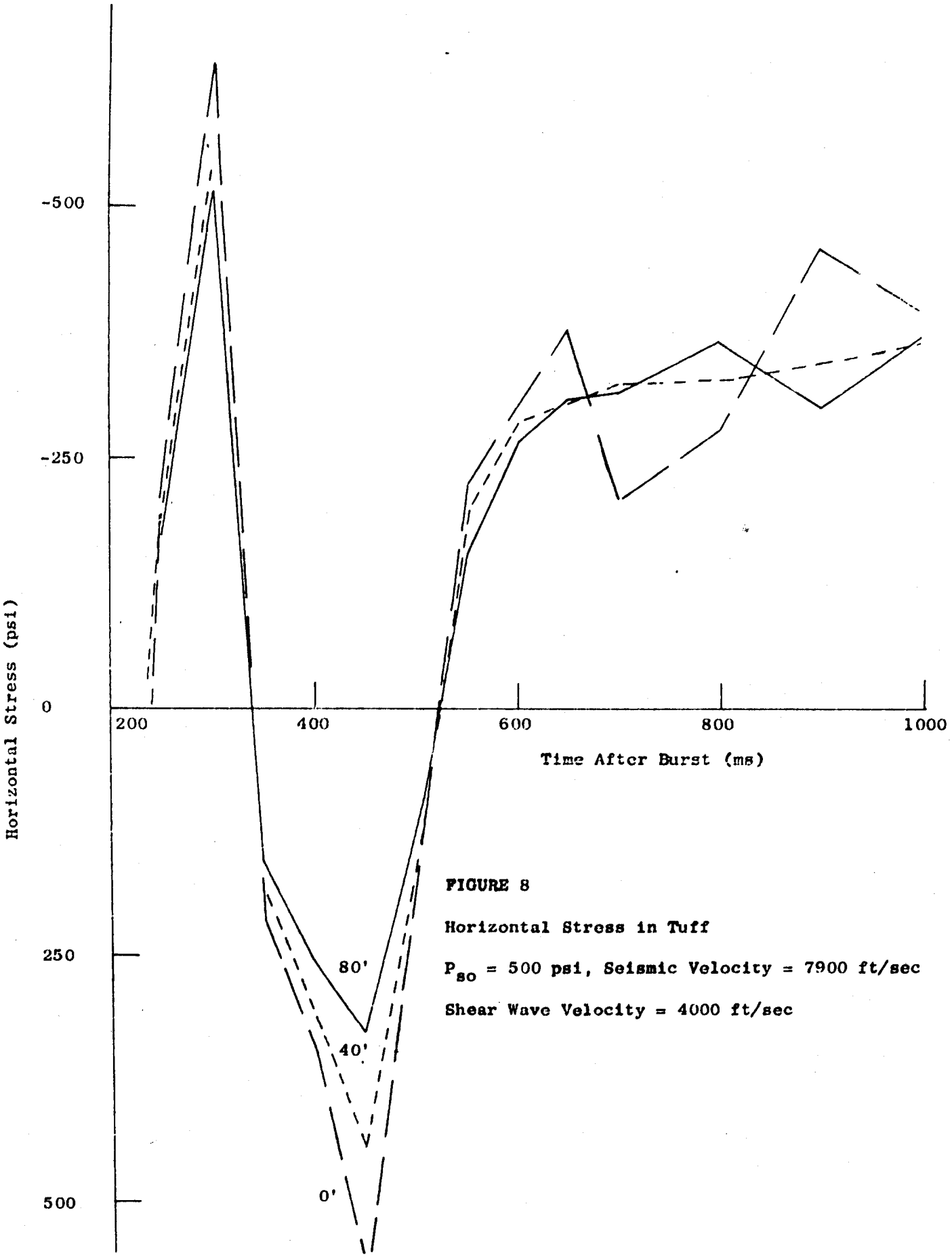

FIGURE 8

Horizontal Stress in Tuff

P_{so} = 500 psi, Seismic Velocity = 7900 ft/sec

Shear Wave Velocity = 4000 ft/sec

FIGURE 9

Shear Stress in Tuff

P_{so} = 500 psi, Seismic Velocity = 7,900 ft/sec

Shear Wave Velocity = 4,000 ft/sec

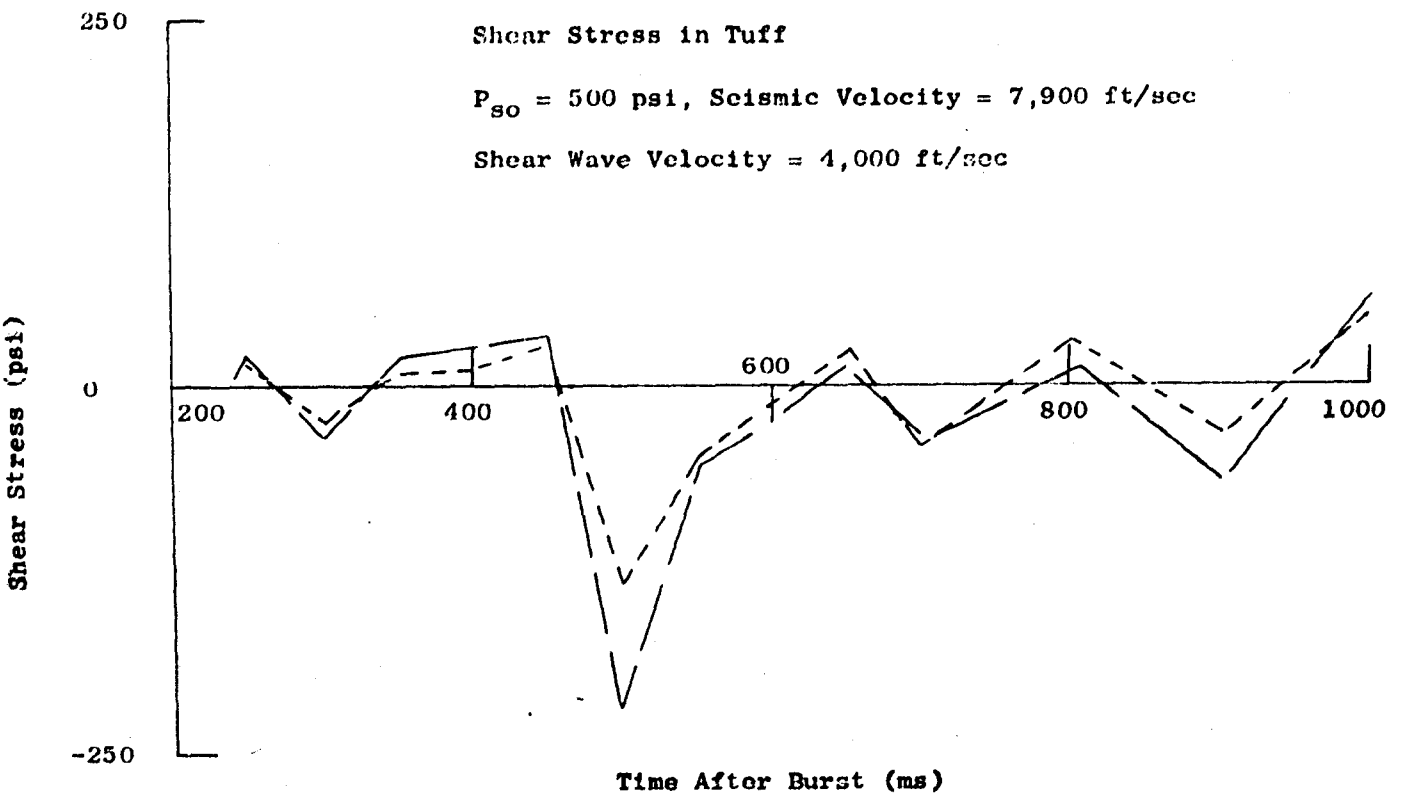

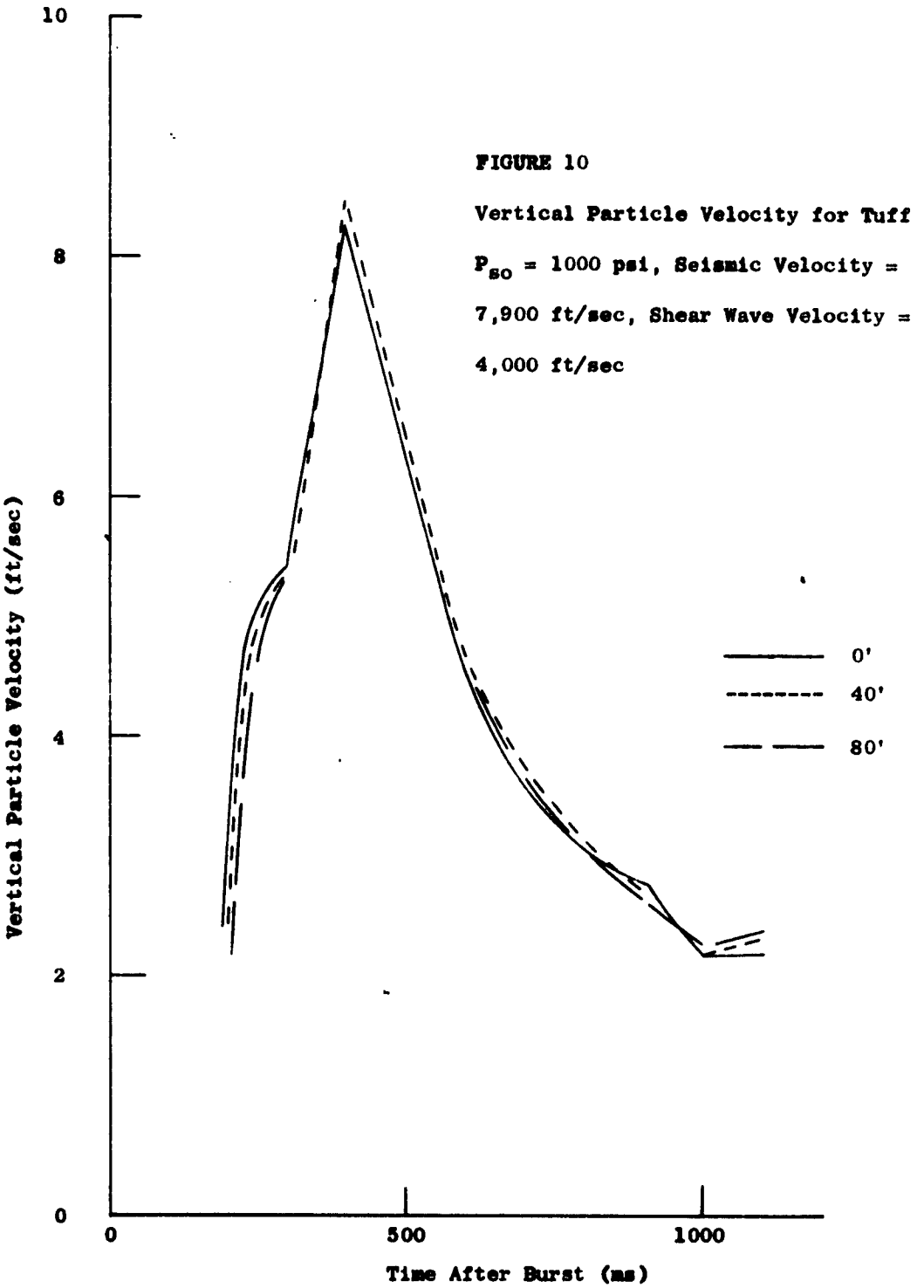

FIGURE 10

Vertical Particle Velocity for Tuff

P_{so} = 1000 psi, Seismic Velocity = 7,900 ft/sec, Shear Wave Velocity = 4,000 ft/sec

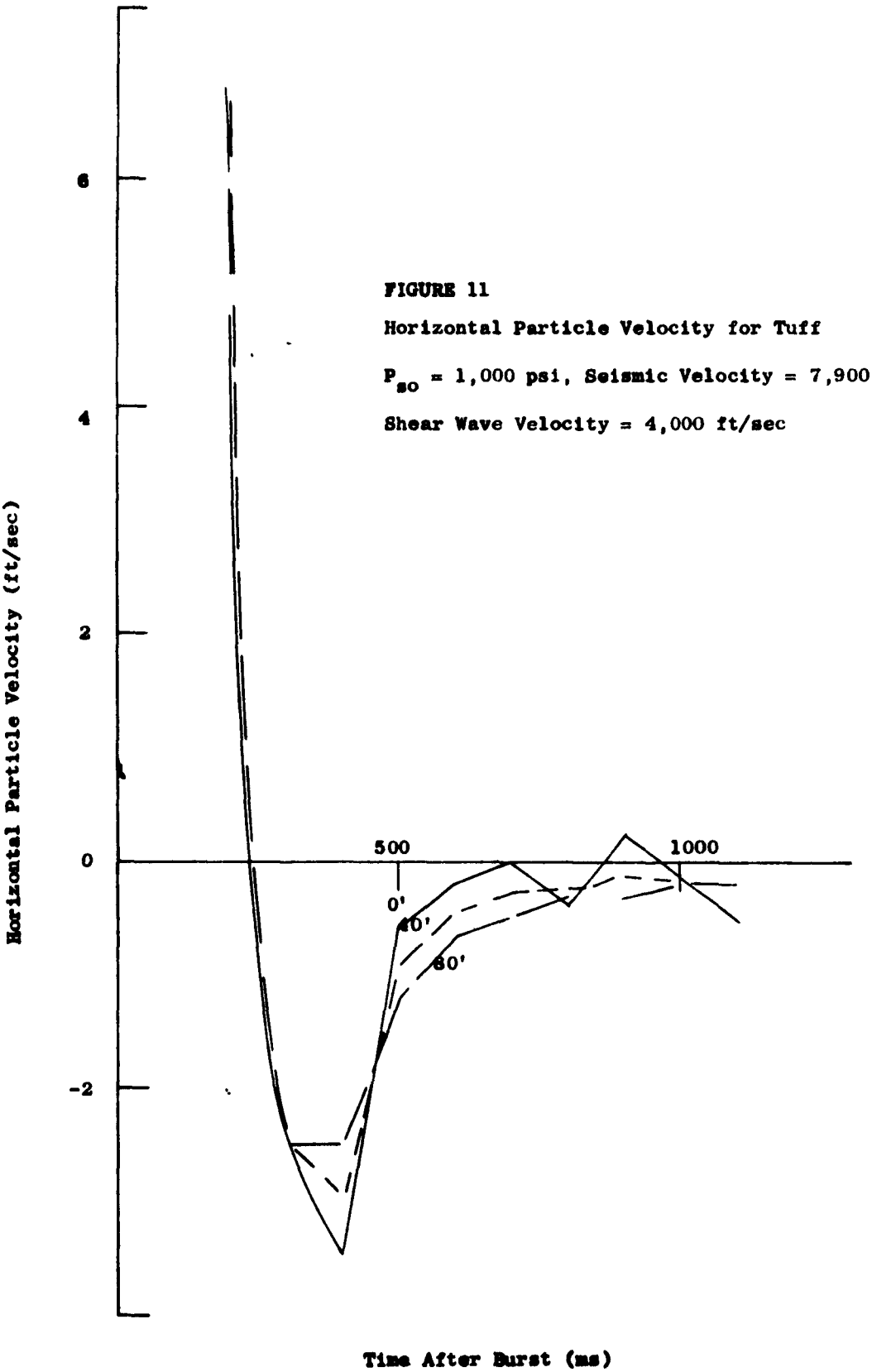

FIGURE 11

Horizontal Particle Velocity for Tuff

P_{so} = 1,000 psi, Seismic Velocity = 7,900 ft/sec

Shear Wave Velocity = 4,000 ft/sec

FIGURE 12

Particle Motions for Surface Points in Tuff at Various Overpressures.
Seismic Velocity = 7,900 ft/sec,
Shear Wave Velocity = 4,000 ft/sec.

P_{so} (psi)	500	1,000	5,000	10,000
Scale:	1/8" = 1'	1/8" = 1'	1/4" = 1'	1/4" = 1'

Arrows mark approximate end of Rayleigh wave disturbances.

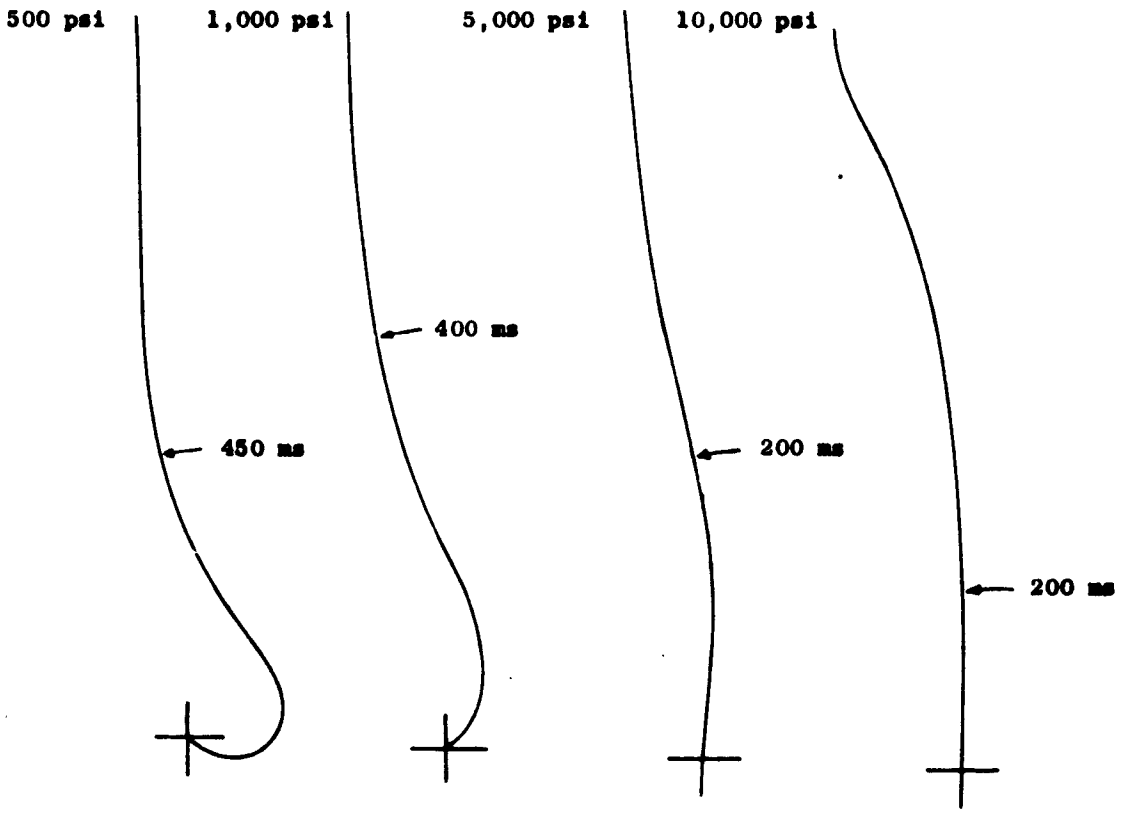

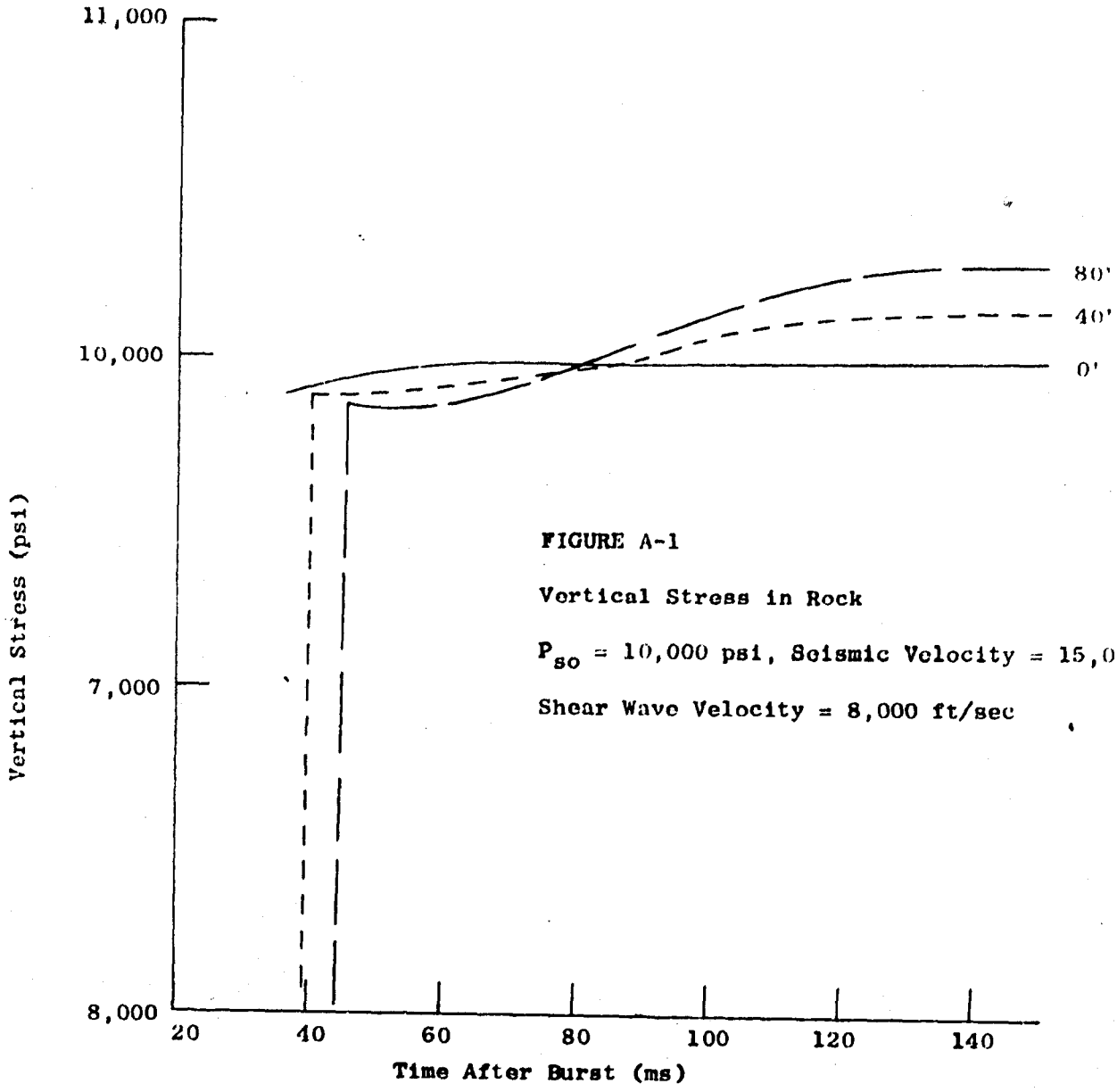

FIGURE A-1

Vertical Stress in Rock

P_{so} = 10,000 psi, Seismic Velocity = 15,000 ft/sec

Shear Wave Velocity = 8,000 ft/sec

FIGURE A-2

Vertical Stress in Rock

P_{so} = 5,000 psi, Seismic Velocity = 15,000 ft/sec

Shear Wave Velocity = 8,000 ft/sec

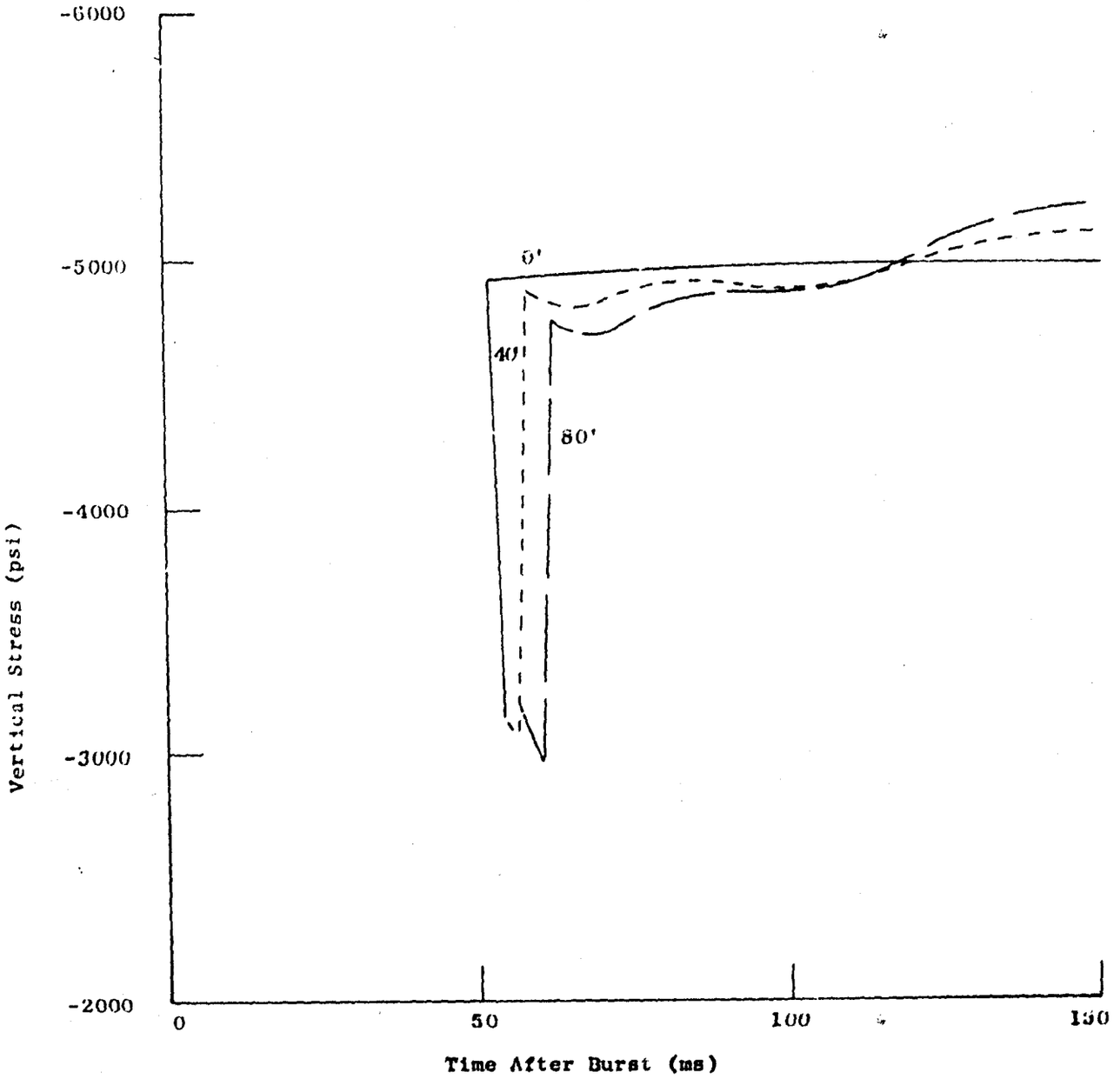

FIGURE A-3

Vertical Stress in Rock

P_{so} = 1,000 psi, Seismic Velocity = 15,000 ft/sec

Shear Wave Velocity 8,000 ft/sec

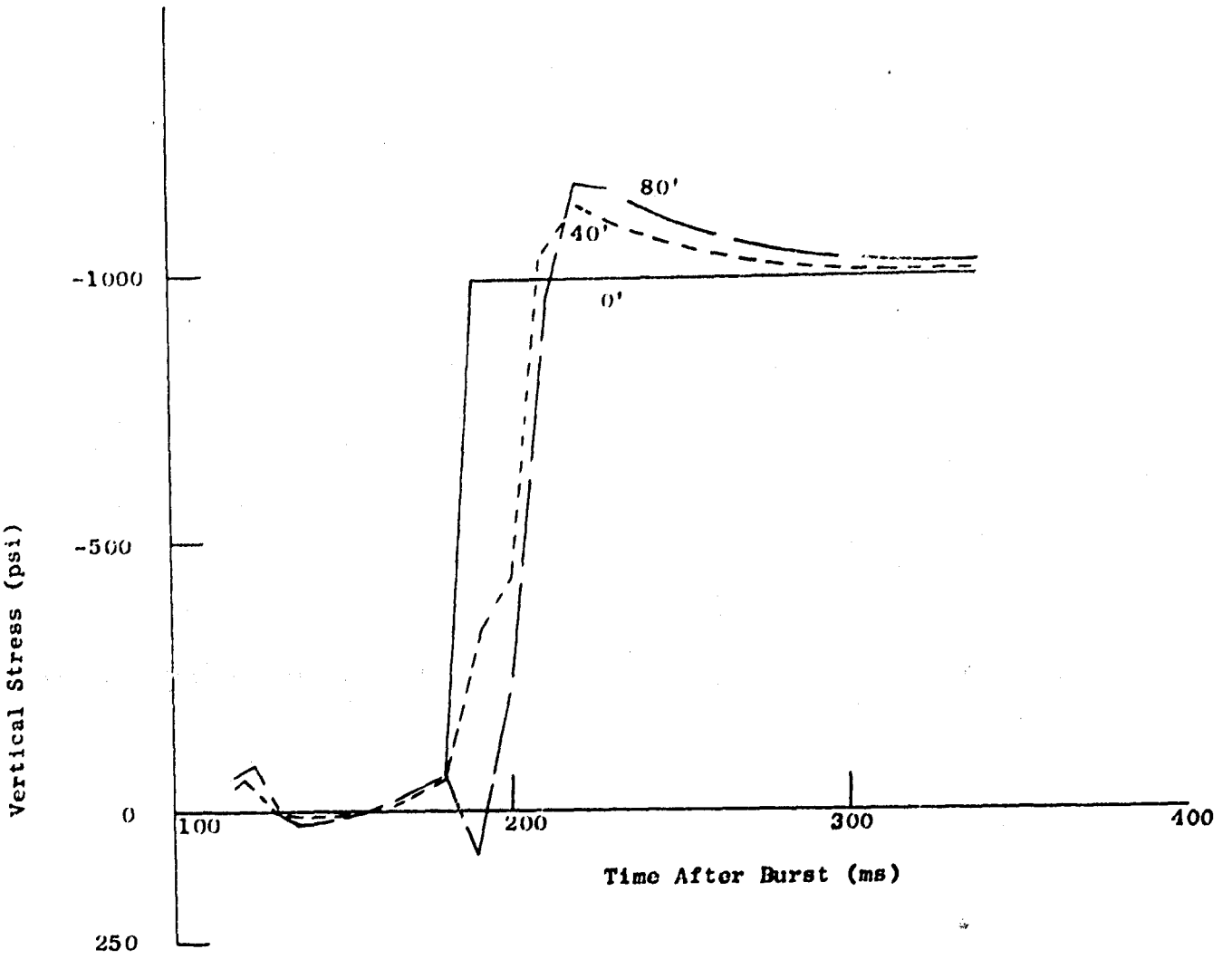

FIGURE A-4

Vertical Stress in Rock

P_{so} = 500 psi, Seismic Velocity = 15,000 ft/sec

Shear Wave Velocity = 8,000 ft/sec

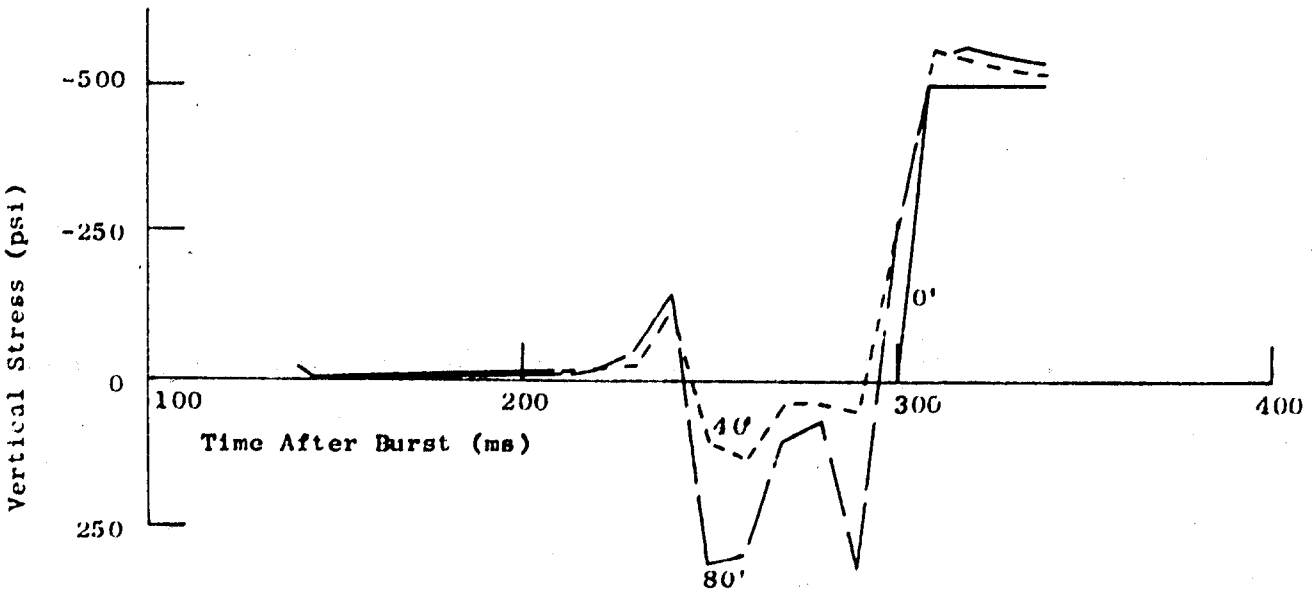

FIGURE A-5

Horizontal Stress in Rock

P_{so} = 10,000 psi, Seismic Velocity = 15,000 ft/sec

Shear Wave Velocity = 8,000 ft/sec

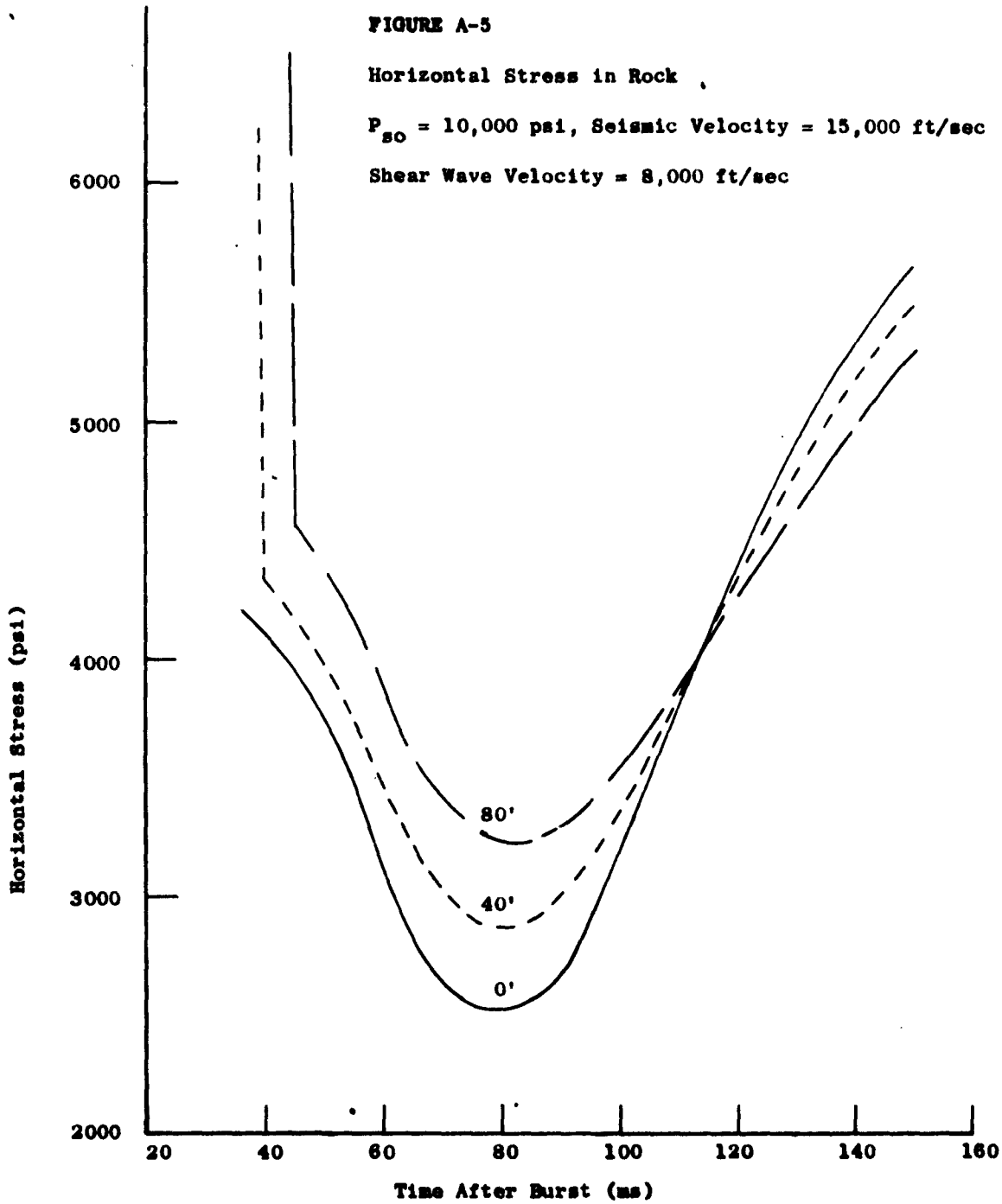

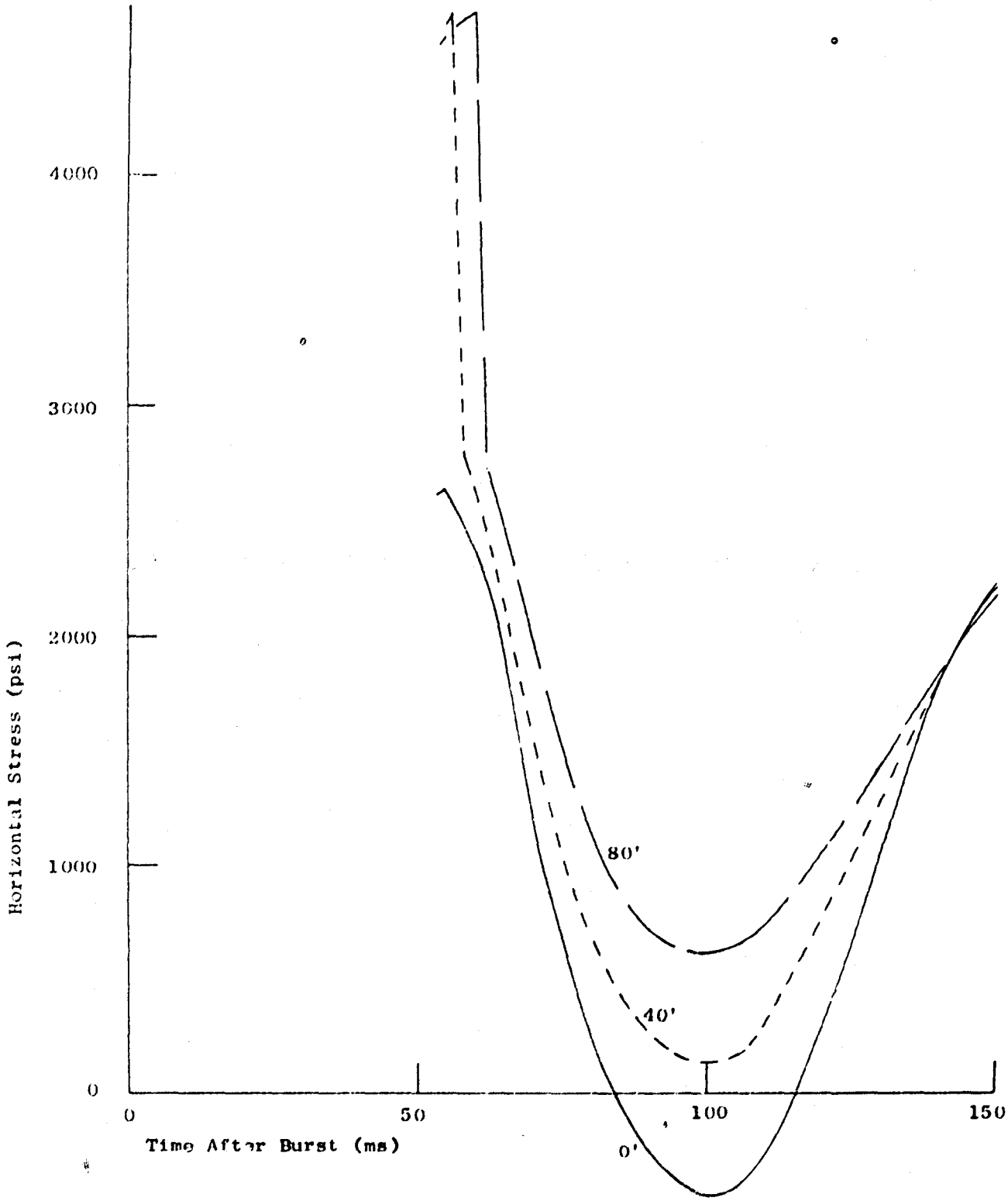

FIGURE A-6

Horizontal Stress in Rock

P_{so} = 5,000 psi, Seismic Velocity = 15,000 ft/sec

Shear Wave Velocity = 8,000 ft/sec

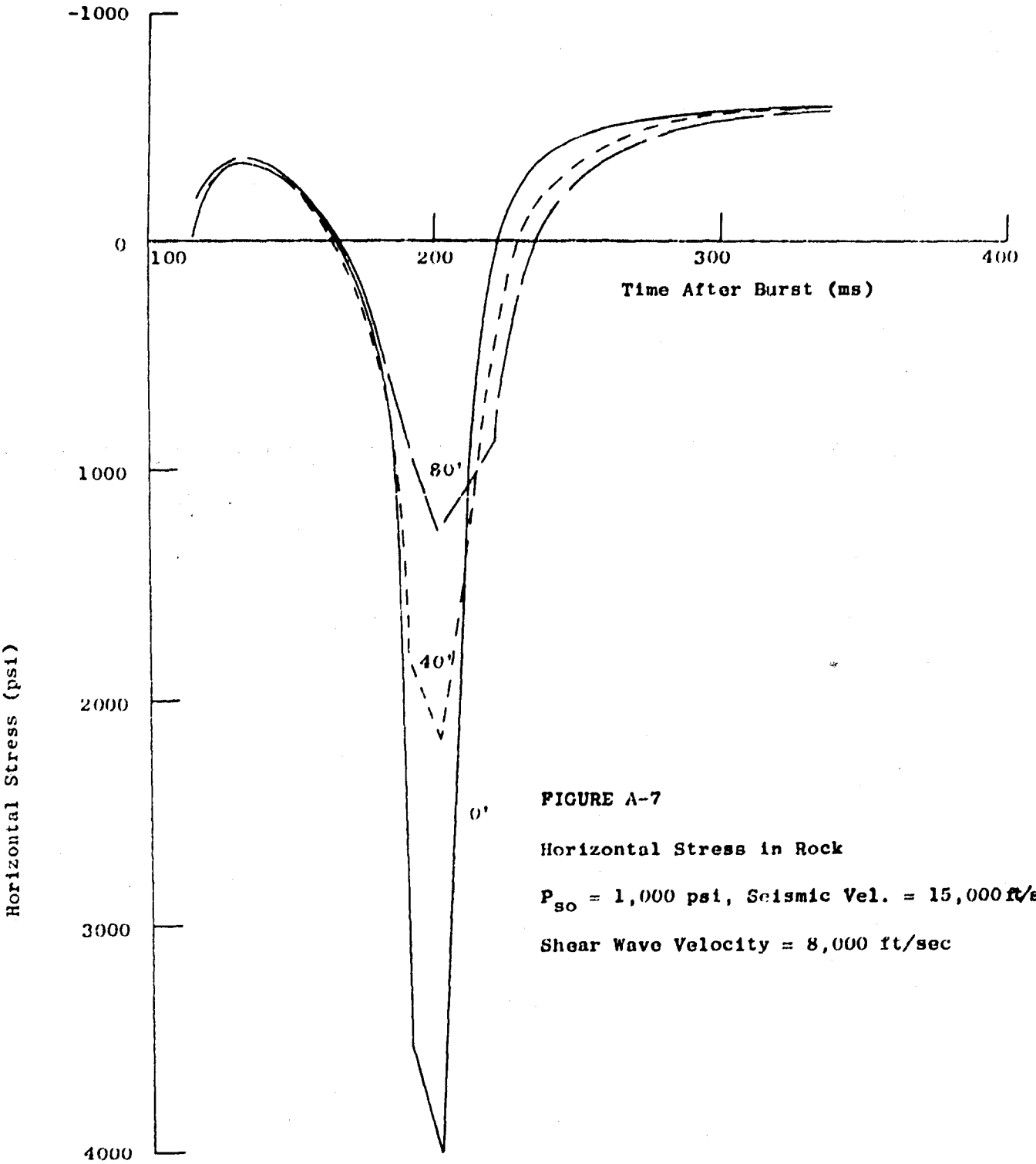

FIGURE A-7

Horizontal Stress in Rock

P_{so} = 1,000 psi, Seismic Vel. = 15,000 ft/sec

Shear Wave Velocity = 8,000 ft/sec

FIGURE A-8

Horizontal Stress in Rock

P_{so} = 500 psi, Seismic Velocity = 15,000 ft/sec

Shear Wave Velocity = 8,000 ft/sec

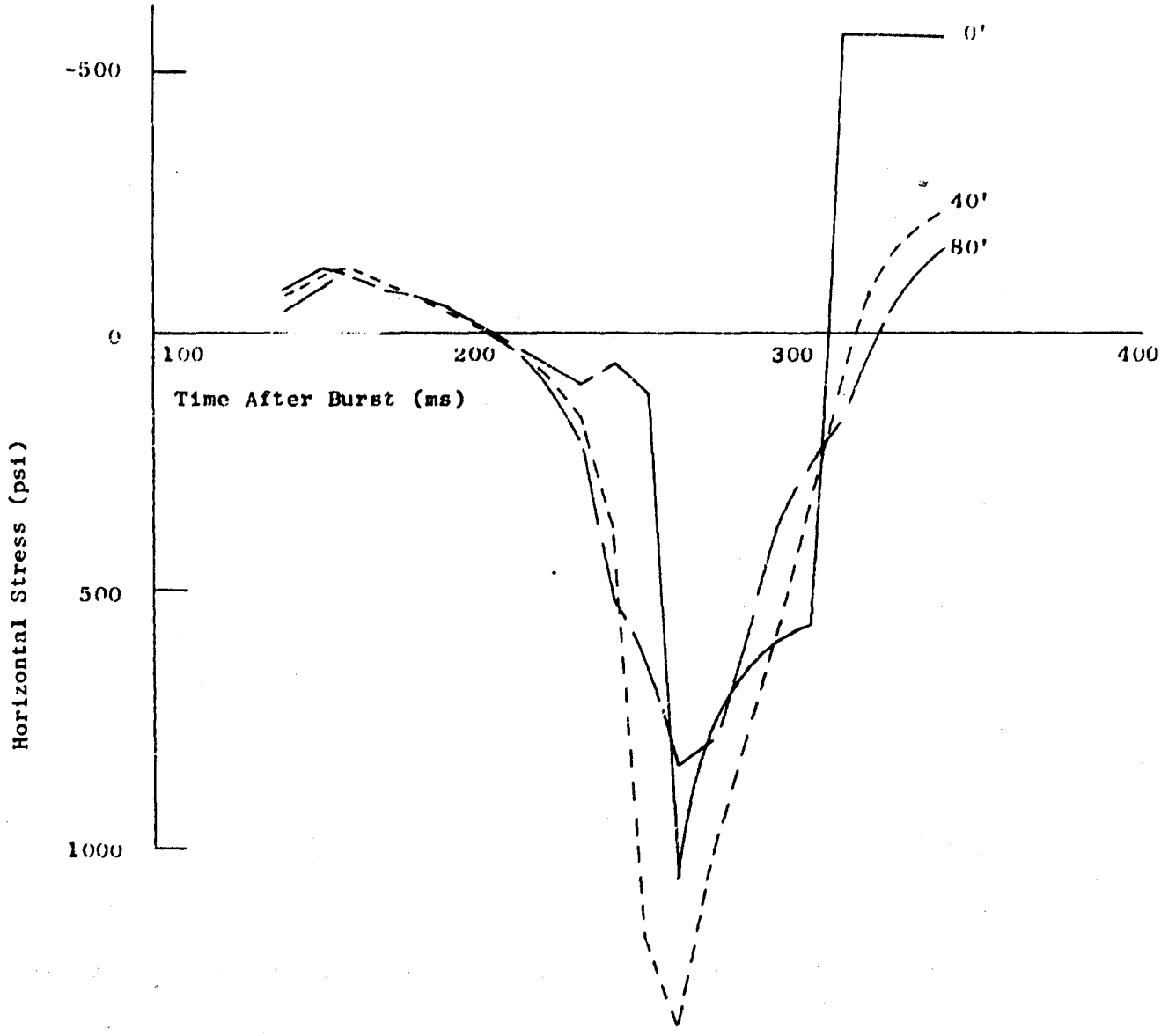

FIGURE A-9

Vertical Particle Velocity for Rock

P_{so} = 1,000 psi, Seismic Velocity = 15,000 ft/sec

Shear Wave Velocity = 8,000 ft/sec

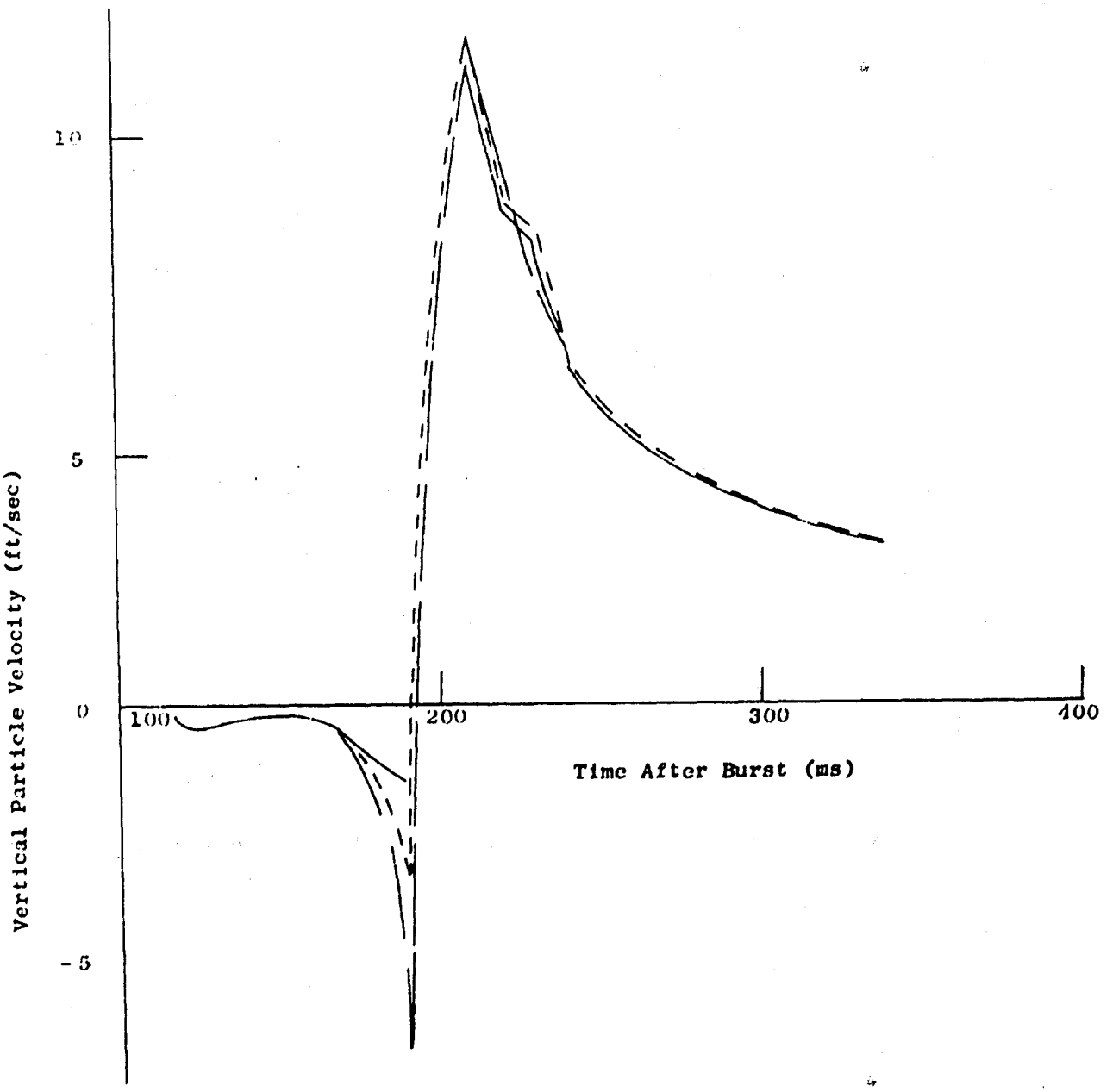

FIGURE A-10

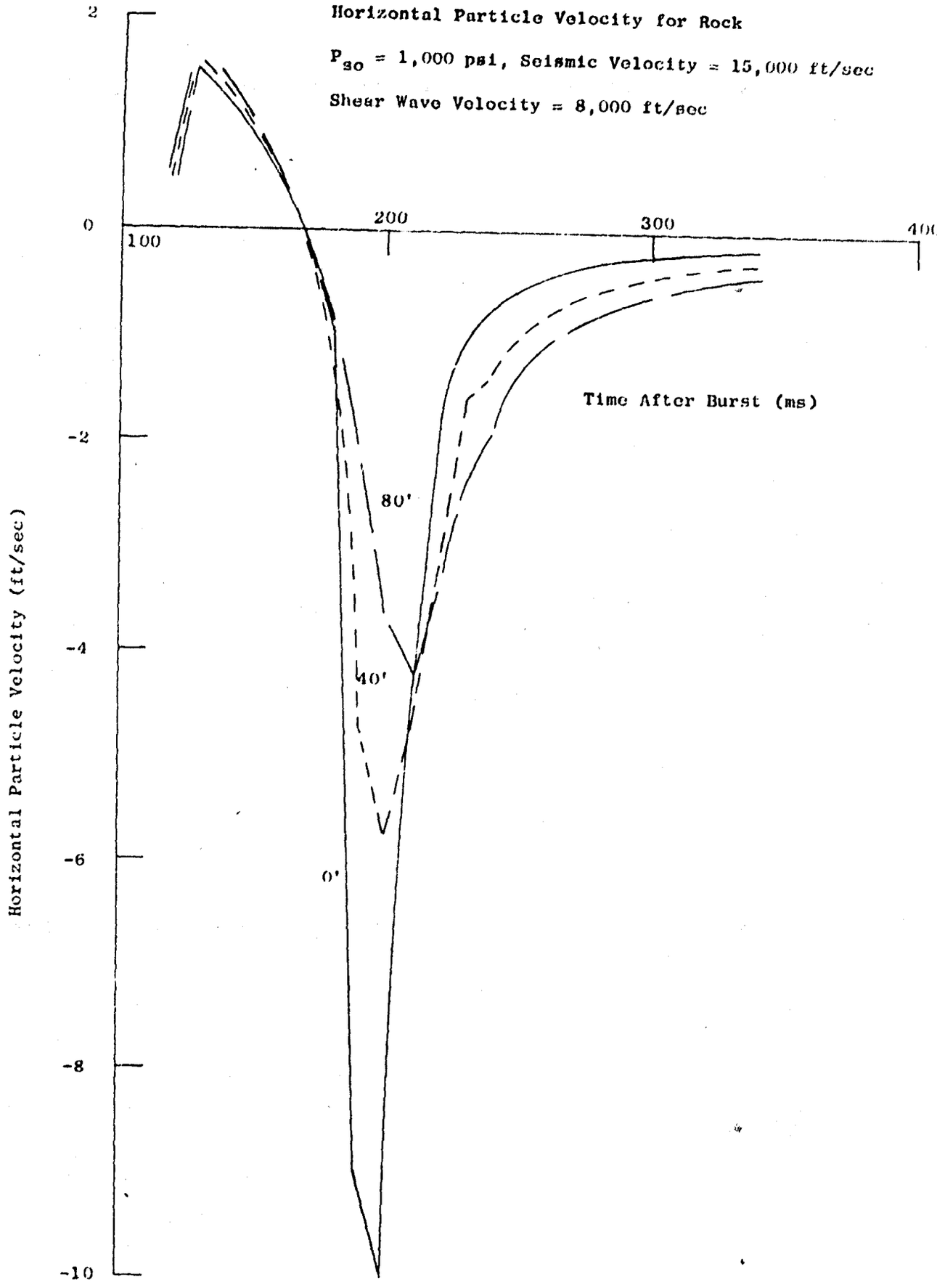
Horizontal Particle Velocity for Rock
P_{so} = 1,000 psi, Seismic Velocity = 15,000 ft/sec
Shear Wave Velocity = 8,000 ft/sec
2
0
-2
-4
-6
-8
-10
100
200
300
400
Time After Burst (ms)
Horizontal Particle Velocity (ft/sec)
80'
40'
0'

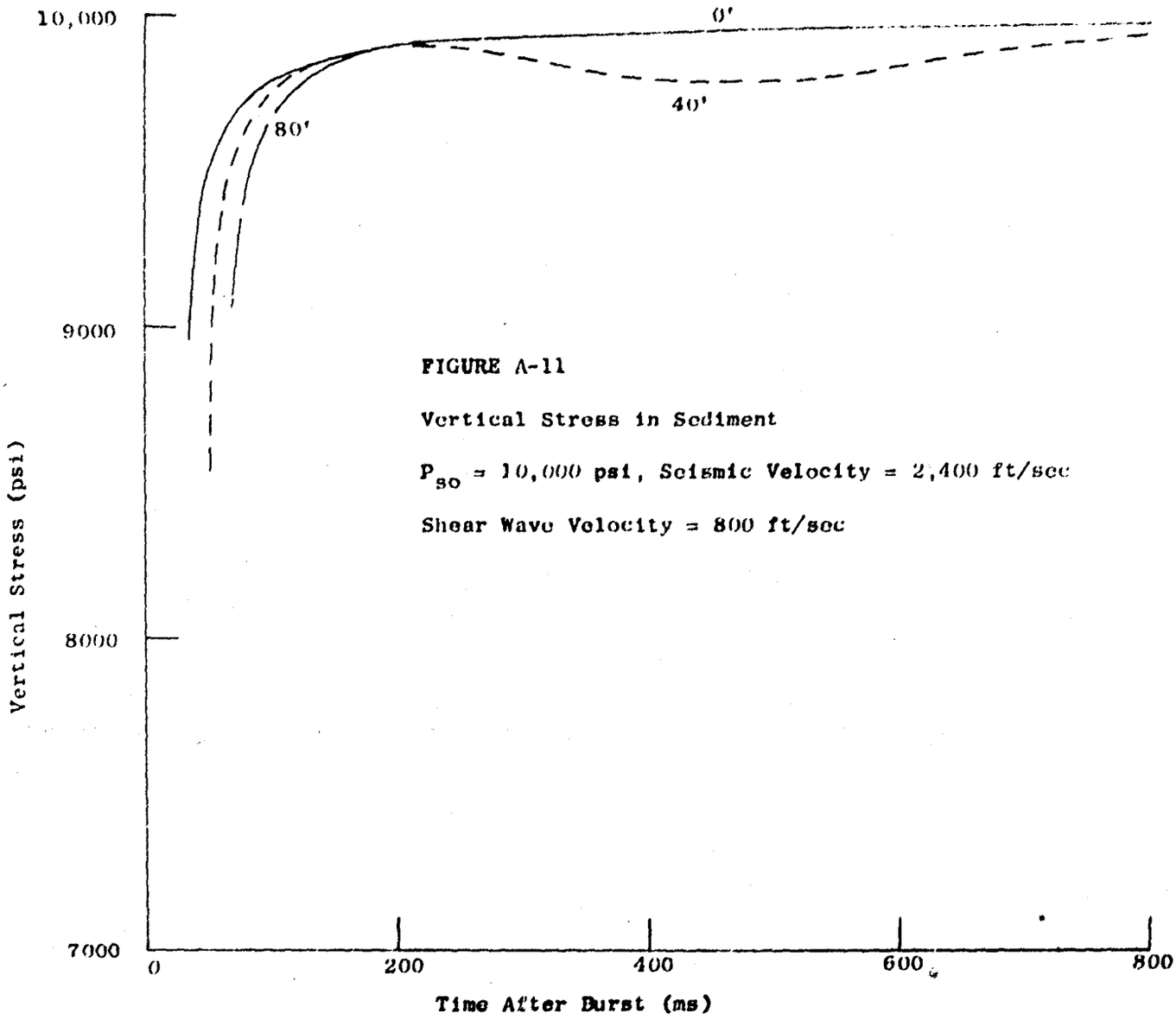

FIGURE A-11

Vertical Stress in Sediment

P_{so} = 10,000 psi, Seismic Velocity = 2,400 ft/sec

Shear Wave Velocity = 800 ft/sec

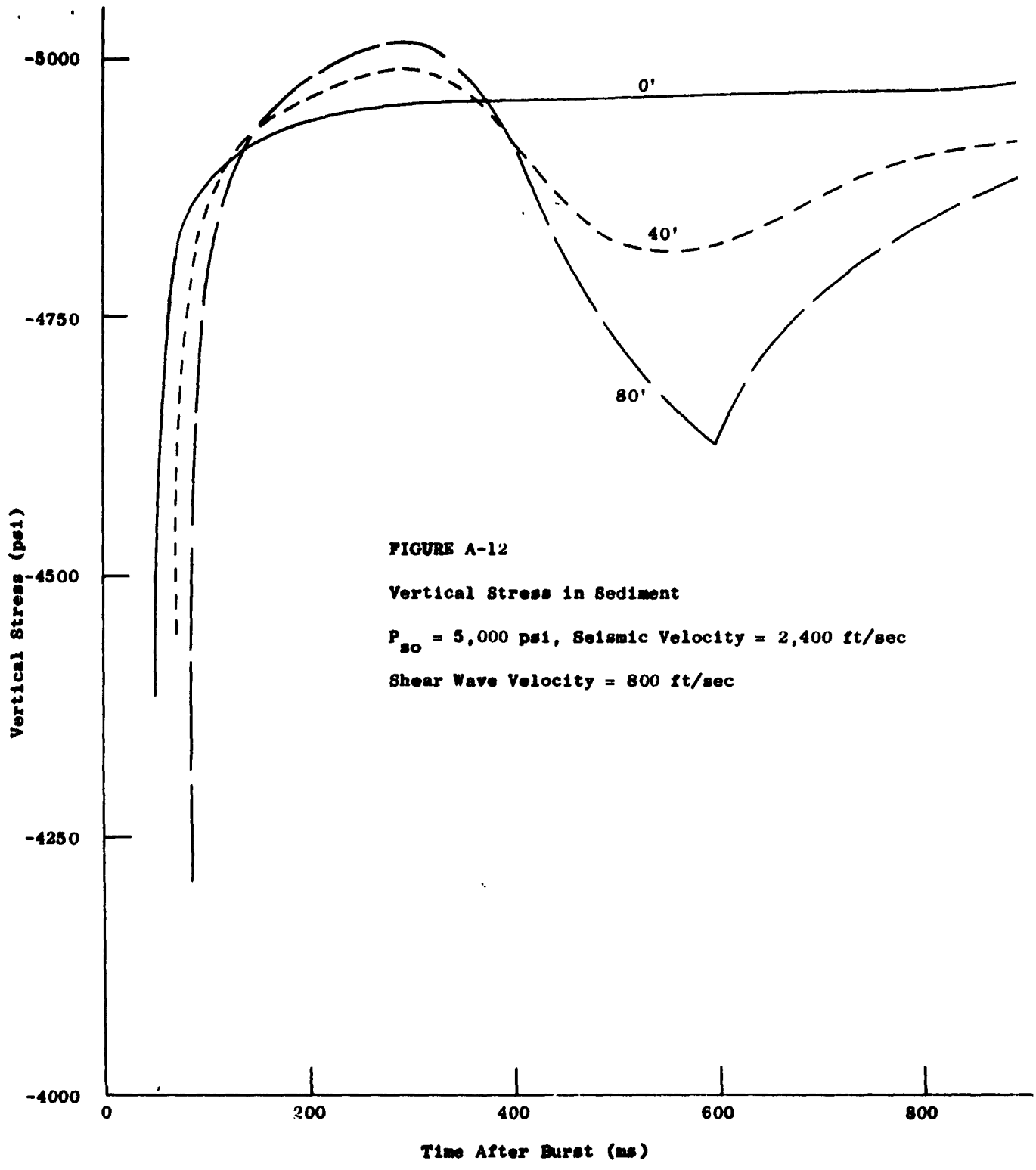

FIGURE A-12

Vertical Stress in Sediment

P_{so} = 5,000 psi, Seismic Velocity = 2,400 ft/sec

Shear Wave Velocity = 800 ft/sec

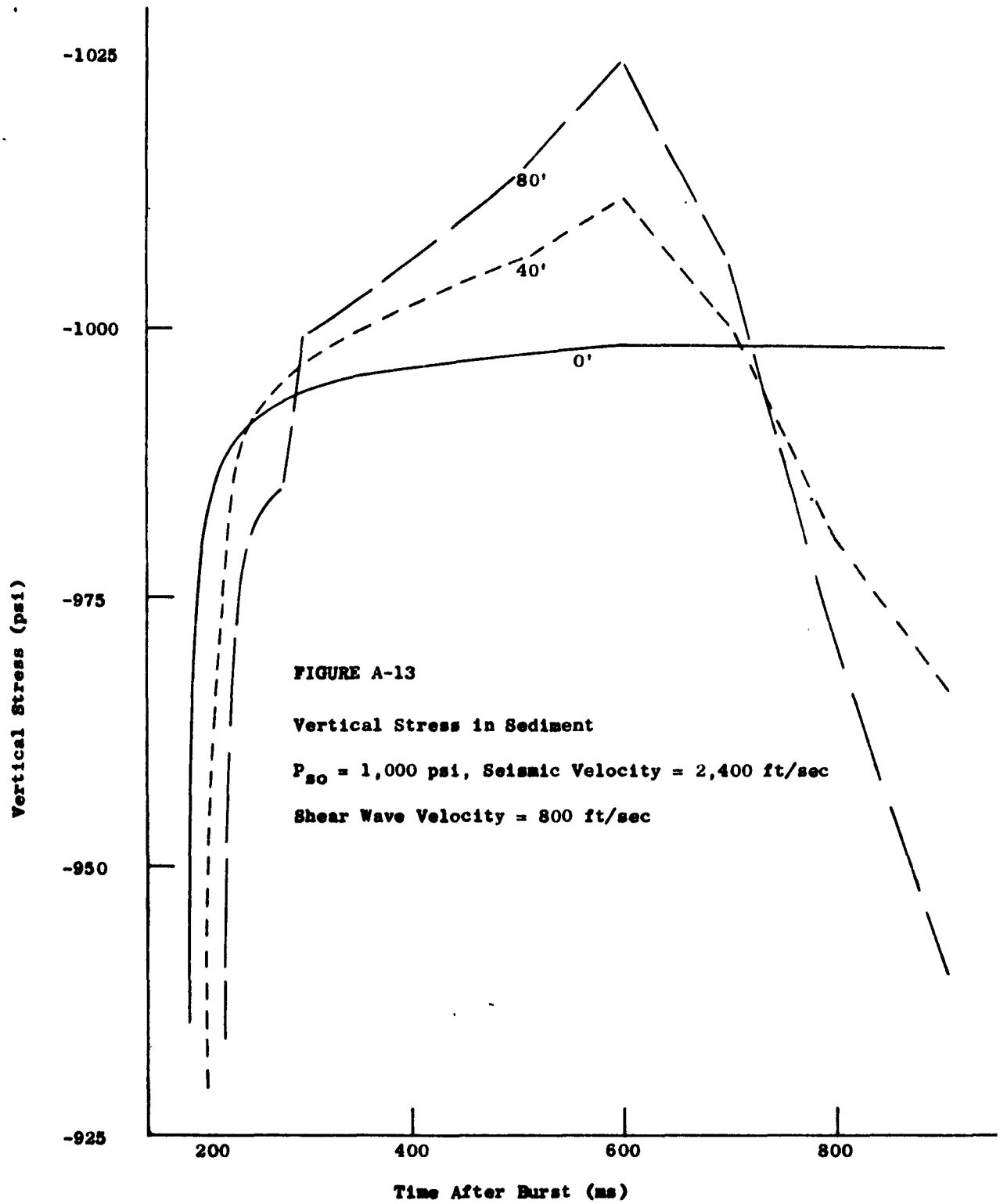

FIGURE A-13

Vertical Stress in Sediment

P_{so} = 1,000 psi, Seismic Velocity = 2,400 ft/sec

Shear Wave Velocity = 800 ft/sec

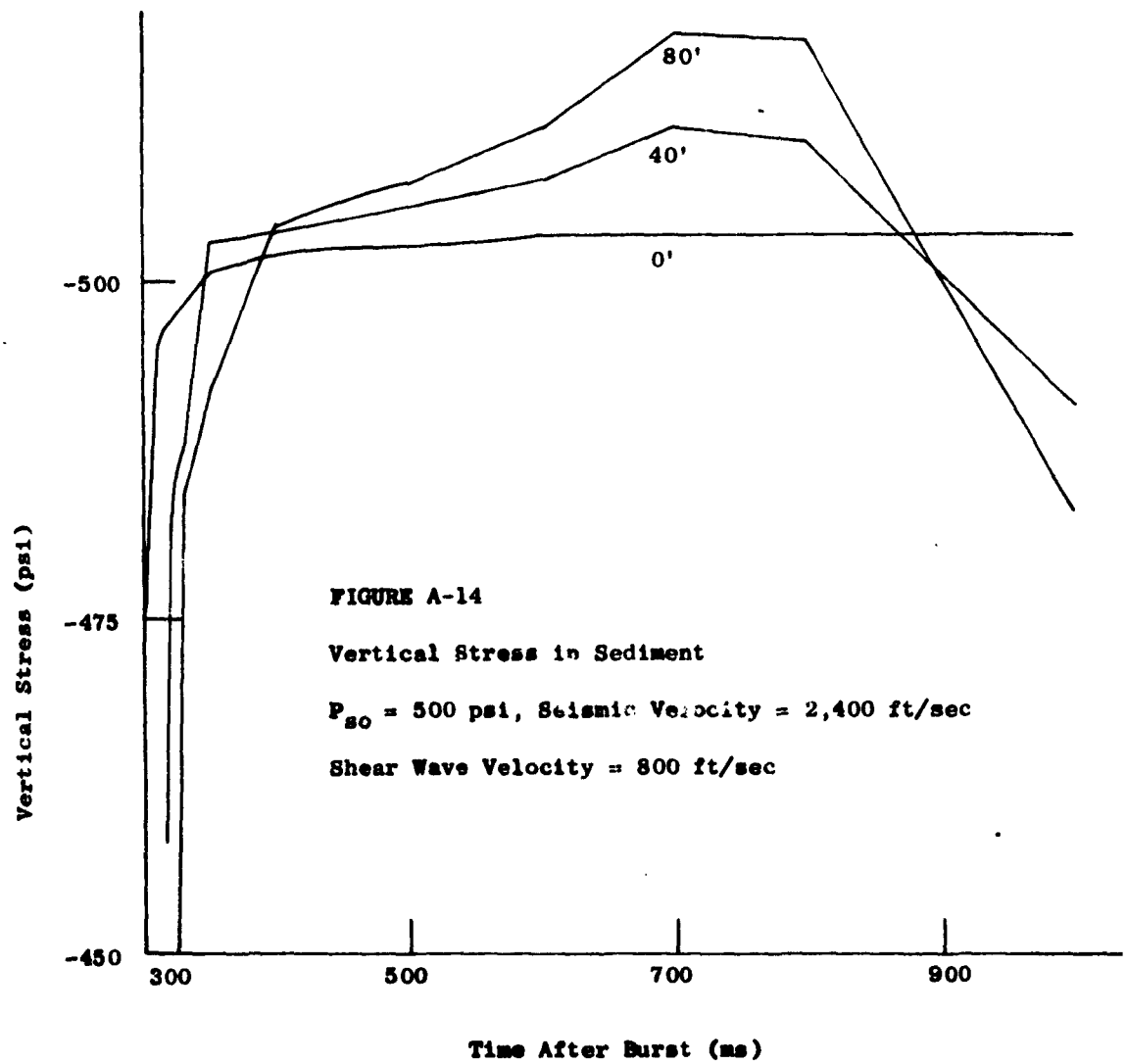

FIGURE A-14

Vertical Stress in Sediment

P_{so} = 500 psi, Seismic Velocity = 2,400 ft/sec

Shear Wave Velocity = 800 ft/sec

FIGURE A-15

Horizontal Stress in Sediment

P_{so} = 10,000 psi, Seismic Velocity = 2,400 ft/sec

Shear Wave Velocity = 800 ft/sec

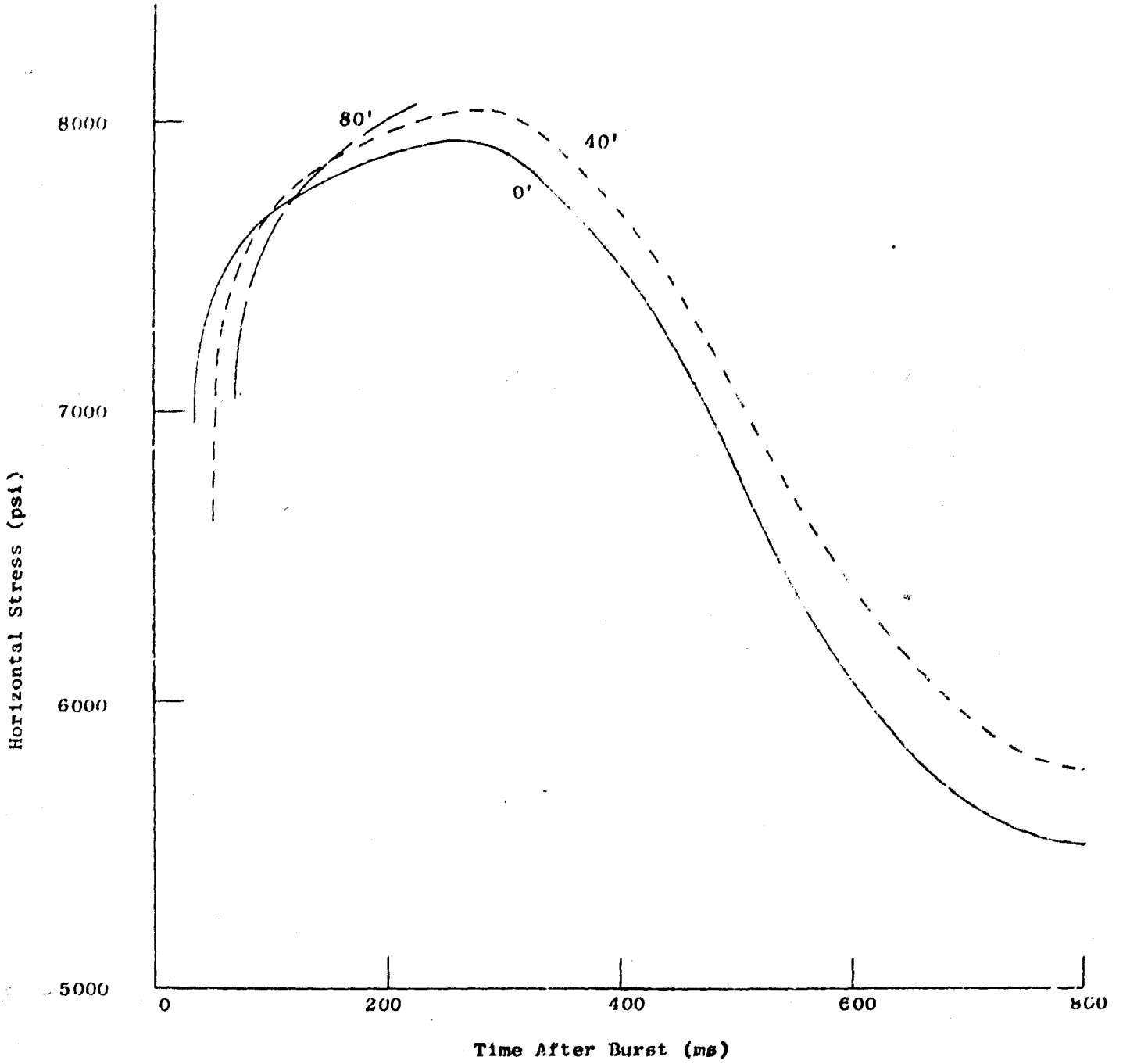

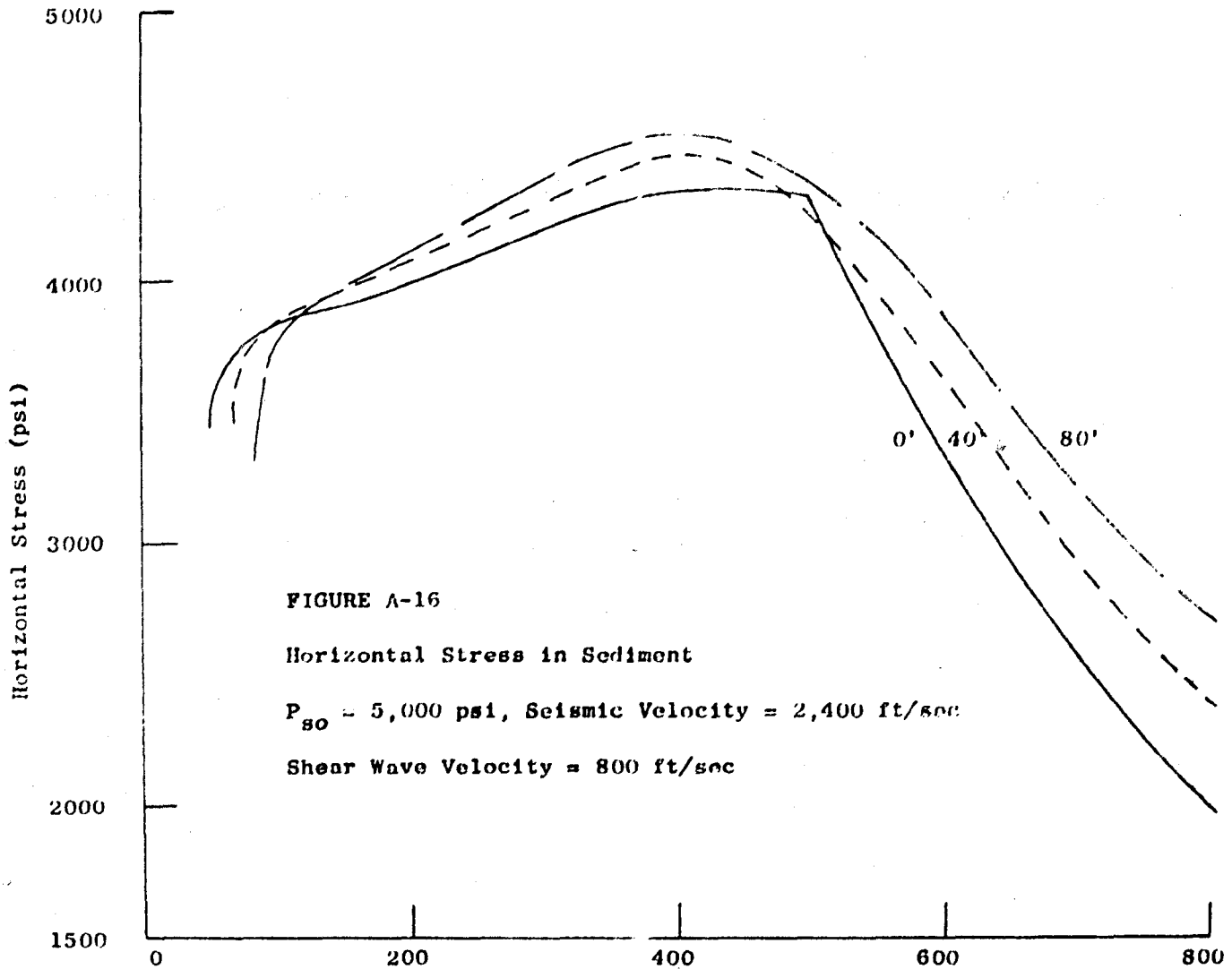

FIGURE A-16

Horizontal Stress in Sediment

P_{so} = 5,000 psi, Seismic Velocity = 2,400 ft/sec

Shear Wave Velocity = 800 ft/sec

FIGURE A-17

Horizontal Stress in Sediment

P_{so} = 1,000 psi, Seismic Velocity = 2,400 ft/sec

Shear Wave Velocity = 800 ft/sec

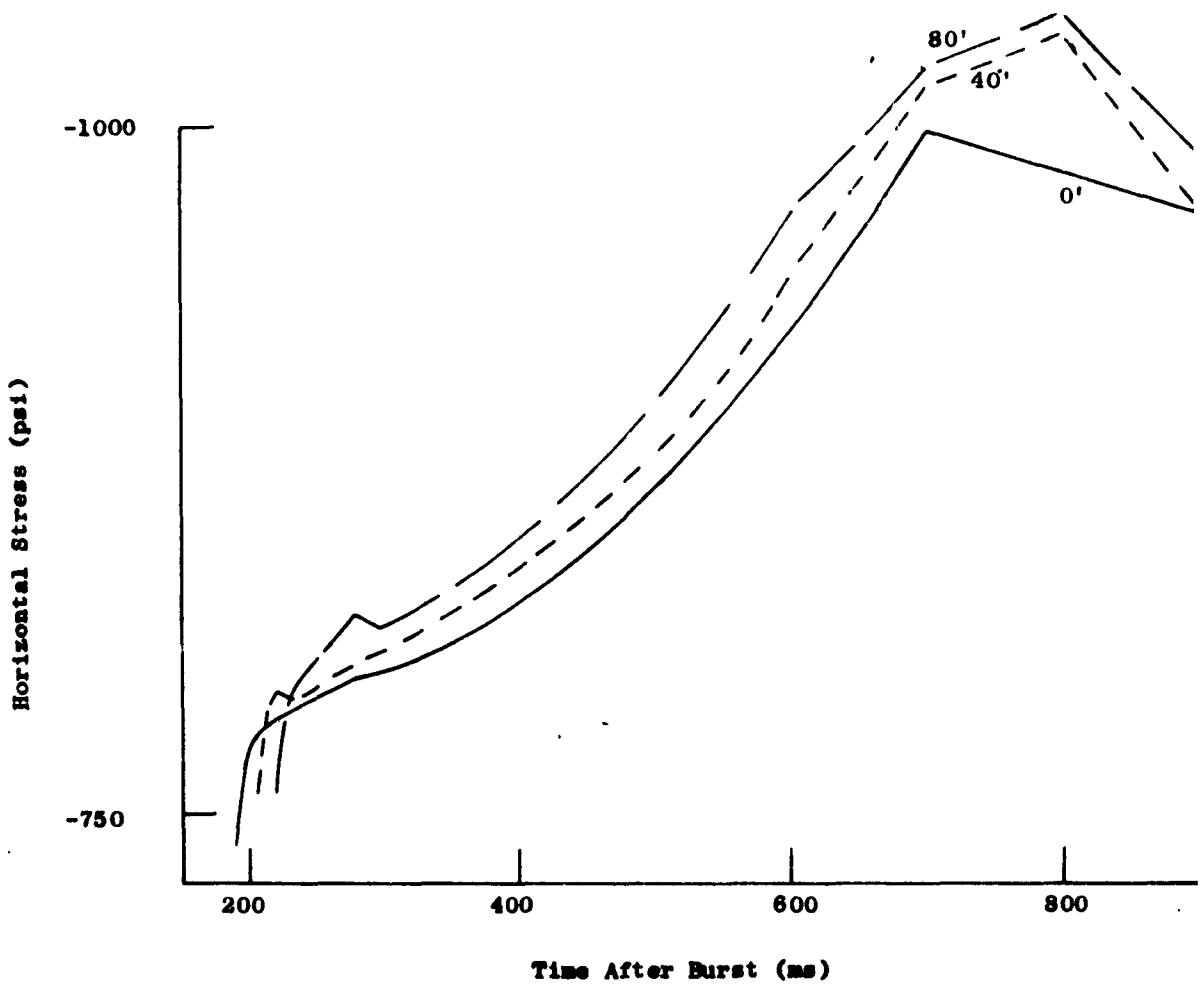

FIGURE A-18

Horizontal Stress in Sediment

P_{so} = 500 psi, Seismic Velocity = 2,400 ft/sec

Shear Wave Velocity = 800 ft/sec

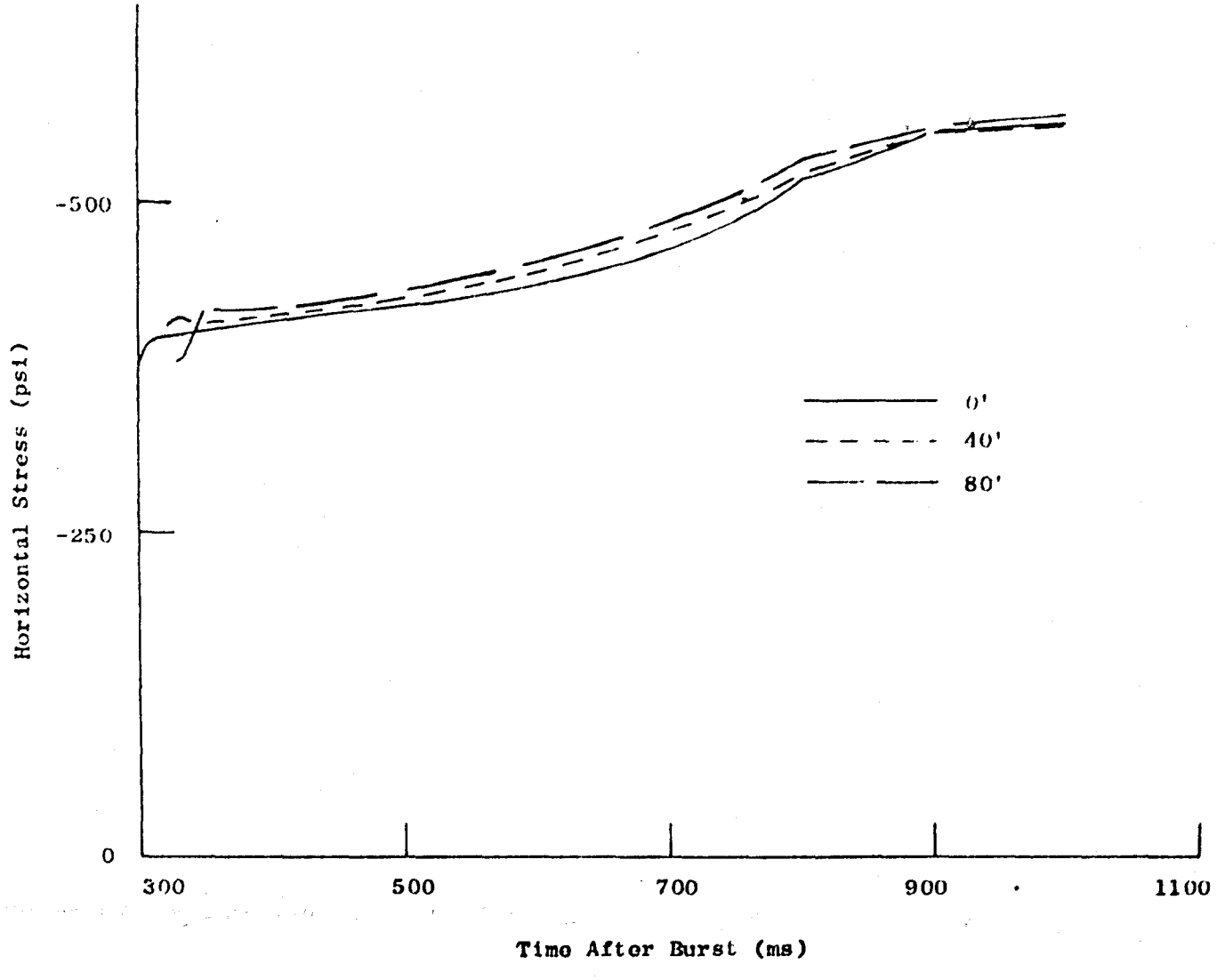

FIGURE A-19

Vertical Particle Velocity for Sediment

P_{so} = 1,000 psi, Seismic Velocity = 2,400 ft/sec

Shear Wave Velocity = 800 ft/sec

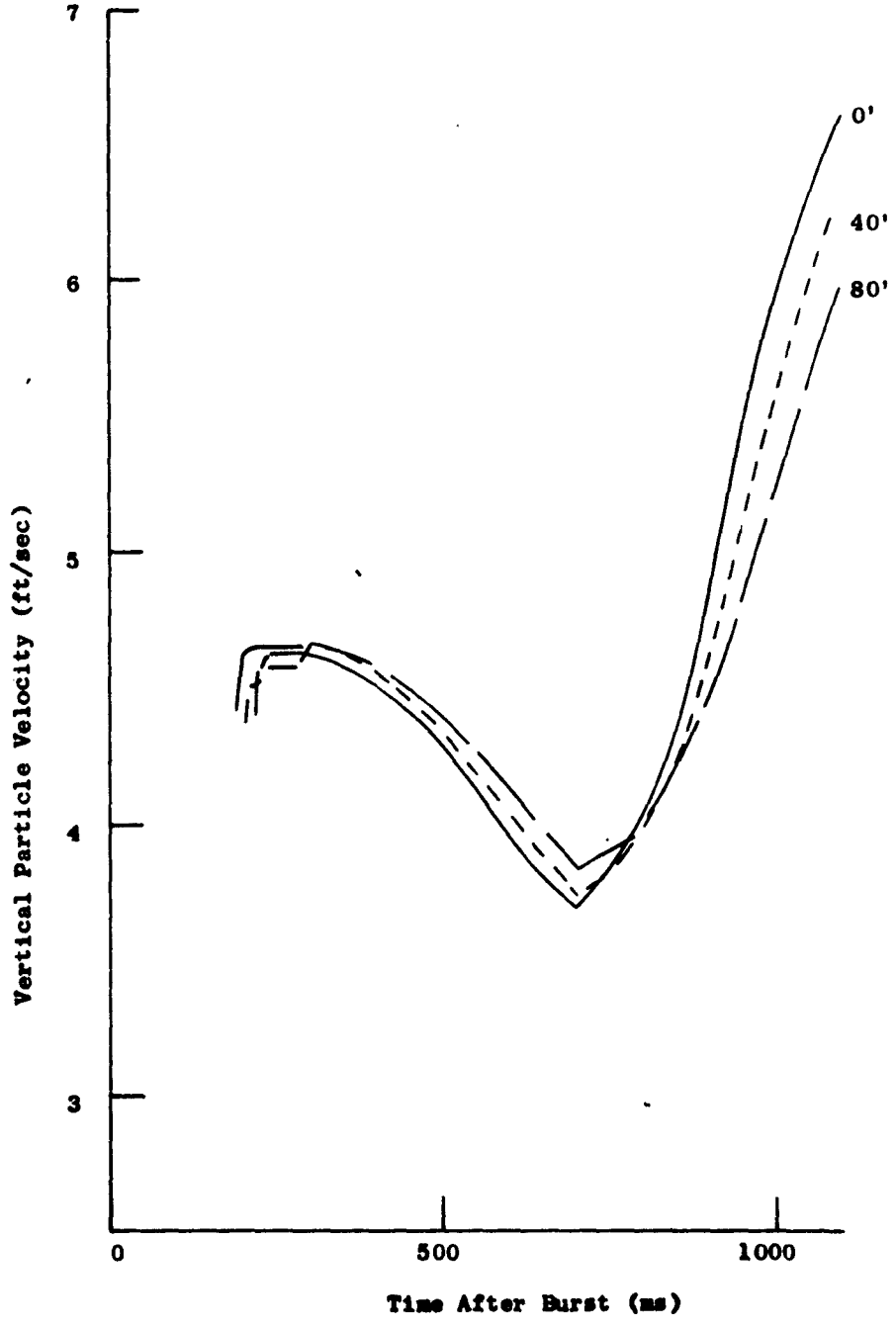

FIGURE A-20

Horizontal Particle Velocity for Sediment

P_{so} = 1,000 psi, Seismic Velocity = 2,400 ft/sec

Shear Wave Velocity = 800 ft/sec